Taylor & Francis
Taylor & Francis Group

RESEARCH PAPER

DNMT1 modulates interneuron morphology by regulating *Pak6* expression through crosstalk with histone modifications

Judit Symmank[a], Cathrin Bayer[a], Christiane Schmidt[a], Anne Hahn[a], Daniel Pensold [ID][a], and Geraldine Zimmer-Bensch [ID][a,b]

[a]Institute of Human Genetics, University Hospital Jena, Jena, Germany; [b]Institute for Biology II, Division of Functional Epigenetics in the Animal Model, RWTH Aachen University, Aachen, Germany

ABSTRACT

Epigenetic mechanisms of gene regulation, including DNA methylation and histone modifications, call increasing attention in the context of development and human health. Thereby, interactions between DNA methylating enzymes and histone modifications tremendously multiply the spectrum of potential regulatory functions. Epigenetic networks are critically involved in the establishment and functionality of neuronal circuits that are composed of gamma-aminobutyric acid (GABA)-positive inhibitory interneurons and excitatory principal neurons in the cerebral cortex. We recently reported a crucial role of the DNA methyltransferase 1 (DNMT1) during the migration of immature POA-derived cortical interneurons by promoting the migratory morphology through repression of *Pak6*. However, the DNMT1-dependent regulation of *Pak6* expression appeared to occur independently of direct DNA methylation. Here, we show that in addition to its DNA methylating activity, DNMT1 can act on gene transcription by modulating permissive H3K4 and repressive H3K27 trimethylation in developing inhibitory interneurons, similar to what was found in other cell types. In particular, the transcriptional control of *Pak6*, interactions of DNMT1 with the Polycomb-repressor complex 2 (PCR2) core enzyme EZH2, mediating repressive H3K27 trimethylations at regulatory regions of the *Pak6* gene locus. Similar to what was observed upon *Dnmt1* depletion, inhibition of EZH2 caused elevated *Pak6* expression levels accompanied by increased morphological complexity, which was rescued by siRNA-mediated downregulation of *Pak6* expression. Together, our data emphasise the relevance of DNMT1-dependent crosstalk with histone tail methylation for transcriptional control of genes like *Pak6* required for proper cortical interneuron migration.

Introduction

The precise balance between excitation and inhibition is crucial for neuronal information processing in the cerebral cortex [1–4], whereby the inhibitory actions of cortical GABAergic interneurons shape and synchronize the responses of excitatory projection neurons [5,6]. Due to their relevance for, circuits, defects in inhibitory interneuron development and function are associated with various neuropsychiatric diseases [4,7–16]. Hence, revealing key regulators that orchestrate cortical interneuron development is crucial to reveal critical events that lead to cortical dysfunction.

Brain development is a complex process through which immature cortical GABAergic interneurons undergo a prolonged period of post-mitotic differentiation and maturation [5,6,17–21]. The long-range tangential migration from their subpallial sites of origin, including the medial and caudal ganglionic eminences as well as the preoptic area (POA) [22–30], into cortical areas represents a critical developmental step. Proper migration relies on the adaption and preservation of a typical migratory morphology capable for directional adjustments induced by extrinsic cues, as well as the maintenance of their viability [29,31–39]. The orchestration of the underlying complex and dynamic subcellular processes requires flexible gene regulation [40–42].

Epigenetic mechanisms like DNA methylation and histone tail modifications provide in part higher ordered regulatory features allowing

for adaptive gene expression modifying developmental programs in response to external stimuli [40–45]. In addition to cytosine methylation in dividing progenitors, the DNA methylation-dependent and independent functions of the DNA methyltransferase 1 (DNMT1) seem to regulate transcription in developing as well as adult neurons [29,43,44,46].

In this context, we previously reported in Pensold et al. (2016) [29] that DNMT1 promotes the migration and survival of *Hmx3*-expressing cortical interneurons generated in the preoptic area (POA) by repressing *Pak6* expression, coding for a p21-activated serine/threonine protein kinase [47]. Conditional deletion of *Dnmt1* causes increased expression levels of *Pak6*, which are associated with morphological alterations of migrating interneurons characterized by higher cellular complexity and increased cell death rates. This significantly reduces the number of interneurons reaching the cortex [29]. However, the underlying mechanism by which DNMT1 represses *Pak6* gene expression remains unclear and seems independent of direct DNA methylation of the *Pak6* locus or of genes encoding for potential regulatory factors [29]. Hence, we hypothesized a crosstalk of DNMT1 with histone modifying enzymes in mediating the transcriptional silencing of *Pak6* in cortical interneurons, which we addressed in the present study.

Our results suggested a bivalent regulation of *Pak6* by simultaneous association of repressive H3K27me3 and permissive H3K4me3 close to the transcription start site. While the association of H3K4me3 at the *Pak6* gene locus appeared DNMT1-independently regulated, we provided evidence for interactions of DNMT1 with the H3K27-methyltransferase EZH2 in modulating transcriptional. In particular, we found that the DNMT1-dependent establishment of repressive H3K27me3 by EZH2 contributes to the regulation of *Pak6* expression. Thus, our study underlines the importance of the crosstalk between different epigenetic key regulators for transcriptional networks underlying cortical interneuron development.

Results

DNA methylation-independent transcriptional control of DNMT1

Our previous study revealed a prominent role of DNMT1 in promoting cortical interneuron migration and survival through the transcriptional regulation of genes involved in cytoskeletal remodeling and cell death such as *Pak6*, encoding for the p21-activated protein kinase PAK6 [29]. Correlative RNA and MeDIP sequencing on FACS-enriched *Hmx3-Cre/tdTomato/Dnmt1* wild-type (*Dnmt1* WT) and *Hmx3-Cre/tdTomato/Dnmt1 loxP^2* (*Dnmt1* KO) mice at embryonic day (E) 16, when POA-derived interneuron migration takes place [28,29], was performed in a previous study [29]. The results suggested a DNA methylation-independent regulation of *Pak6* expression by DNMT1. Indeed, the majority of genes with altered expression in *Dnmt1*-deficient POA interneurons did not display changes in gene methylation and vice versa (Figure 1(A)). This strongly suggested DNA methylation-independent actions of DNMT1 mediating transcriptional control in developing cortical interneurons, in addition to potential secondary effects of *Dnmt1* deletion. GO analysis of the 1050 genes displaying increased expression without respective changes in DNA methylation in *Dnmt1*-deficient interneurons (obtained from the dataset of Pensold et al., 2016 [29]), resulted in a significant enrichment of membrane and cell shape-associated genes, as well as genes related to protein phosphorylation (Figure 1(B)). In agreement with this, the protein kinase PAK6 is involved in phosphate transfer as well as the regulation of neurite branching in post-mitotic neurons [29,48,49].

Besides cytosine methylation, DNMT1 contributes to the complex epigenetic network of gene regulation by modulating permissive and repressive chemical modifications of amino acids on histone tails via interactions with histone-modifying enzymes [50,51]. As such interactions were already shown to regulate relevant gene transcription in non-neuronal cells [52,53], we next investigated potential alterations in histone modifications after *Dnmt1* deletion.
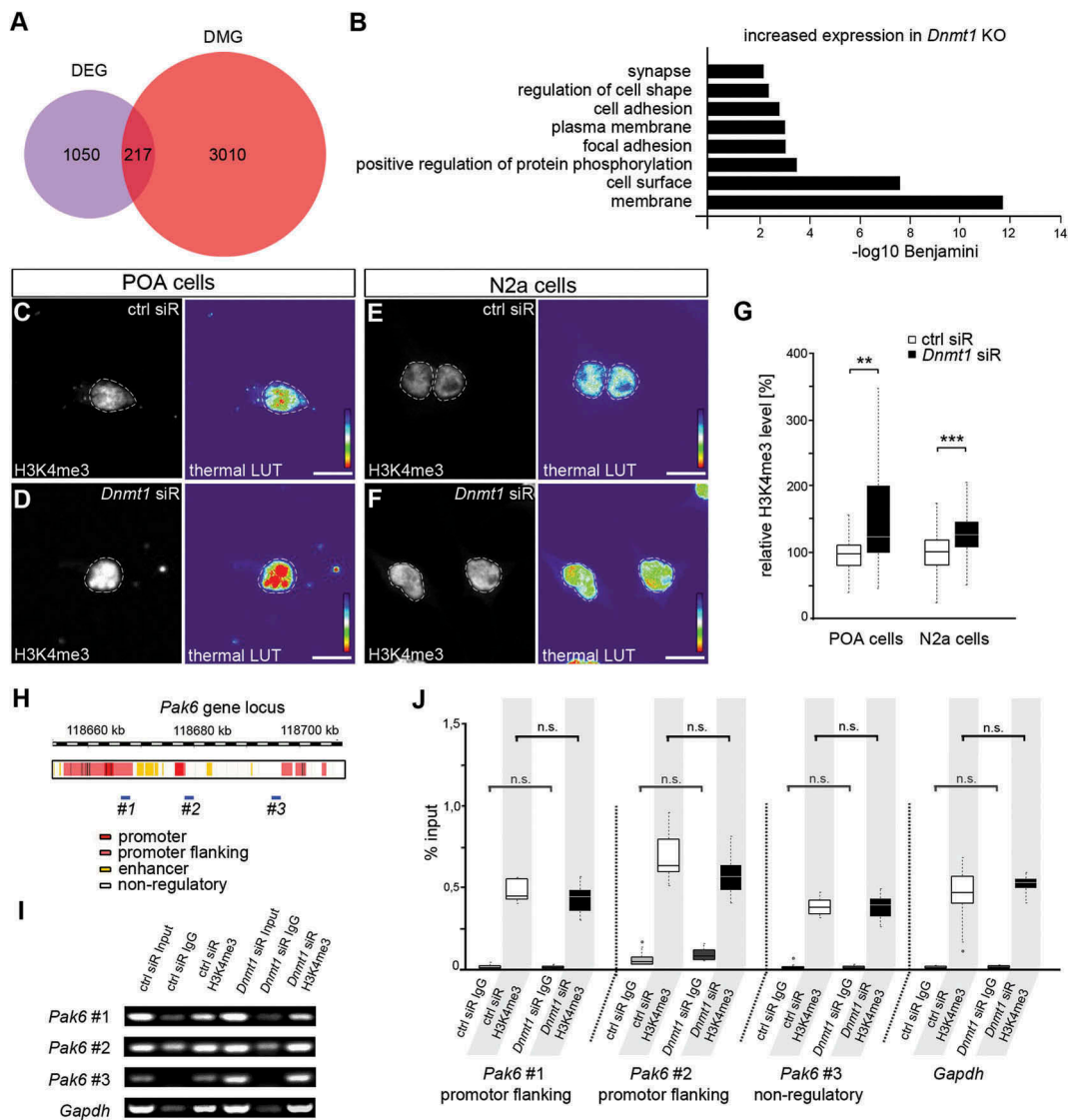
Figure 1. DNA methylation-independent functions of DNMT1. (A) Venn diagram indicating differentially expressed genes (DEG, purple circle) and differentially methylated genes (DMG, red circle) as well as their overlap (magenta) between E16 FACS-enriched *Hmx3-Cre/tdTomato/Dnmt1* wild-type (*Dnmt1* WT) and *Hmx3-Cre/tdTomato/Dnmt1 loxP²* (*Dnmt1* KO) POA cells determined by correlative RNA and MeDIP sequencing. (B) Gene ontology (GO) analysis of genes that were significantly up-regulated in FAC-sorted E16 *Dnmt1*-deleted *Hmx3-Cre/tdTomato* POA cells ($P < 0.05$; Benjamini adjusted, foldchange > 1.3) and which did not display changes in gene methylation compared with E16 *Hmx3-Cre/tdTomato/Dnmt1* wild-type POA cells. (C-G) Representative microphotographs of dissociated E16 (+ 2 DIV) POA cells (C, D) and neuroblastoma (N2a) cells (E, F) treated either to control (C, E) or *Dnmt1* siRNA (D, F), and stained for H3K4me3, shown as fluorescence intensity in black/white code and as thermal color-code (thermal LUT). The mean grey value is quantified relative to controls in G (n = 26 POA and 345 N2a cells for ctrl siRNA, n = 24 POA and 245 N2a cells for *Dnmt1* siRNA). (H) Schematic illustration of the *Pak6* gene locus with promoter (red), promoter flanking (light red), enhancer (yellow) and non-regulatory (white) sites according to UCSC genome browser showing DNA primer positions (#1, #2, #3) in regulatory (#1, #2) and non-regulatory (#3) gene regions. (I, J) ChIP-analysis of control and *Dnmt1* siRNA-treated N2a cells with a specific H3K4me3 antibody reveals the association of H3K4me3 to specific primer locations (#1–3 in H) in the *Pak6* gene (I), analyzed by quantitative PCR and normalized to the amount of input DNA (J; three individual experiments with four technical replicates each). IgG controls were included to determine non-specifically bound DNA. 'n' refers to the number of analyzed cells. **$P < 0.01$; ***$P < 0.001$; Student's t-test. Scale bars: 10 μm in (C-F). Ctrl, control; siR, siRNA; POA, preoptic area.

Global H3K4 trimethylation was increased in Dnmt1-depleted neuronal cells

Modifications at specific residues of histone amino acid tails affect gene accessibility [54–57]. Dependent on the modified lysine residue, histone methylation can either lead to permissive or repressive gene expression states [54–57]. *Dnmt1*-deficient embryonic POA-interneurons displayed transcriptional changes of diverse genes involved in the trimethylation of H3K4, which is associated to permissive chromatin structure. In detail, an increased expression of *Kmt2d* and *Kmt2g* coding for histone-lysine N-methyltransferases (HMT [58–60]) was observed in embryonic FACS-enriched *Hmx3-Cre/tdTomato/Dnmt1* loxP^2 cells (Supp. Figure 1). Both HMTs are classified as trithorax-group proteins with important function in maintaining gene expression and in promoting the methylation of H3K4 [58,59,61]. Mono-, di- and tri-methylation at H3K4, often correlated with enhanced gene transcription, are regulated by MLL-complexes that include the WDR5 protein [62–64]. The stability of WDR5 was reported to be increased by reduced expression of *Cul4b* [65,66], which we also found diminished in *Dnmt1*-deficient POA cells (Supp. Figure 1). Together, the expressional changes detected in *Dnmt1*-deficient interneurons pointed to changes in the H3K4 methylation machinery. Hence, we next asked whether the methylation of H3K4 was altered in *Dnmt1*-deficient cells with potential implications for the DNA methylation-independent transcriptional up-regulation of genes like *Pak6*. For this, we transfected dissociated POA cells isolated from E16 wild-type mice either with control or *Dnmt1* siRNA and performed immunostaining against H3K4me3. Fluorescence intensity measurements indeed showed enhanced global trimethylation of H3K4 in *Dnmt1*-depleted POA cells (Figure 1(C,D,G)), which could be associated to an increase in gene transcription [62–64]. Hence, these data point to a DNMT1-dependent modulation of H3K4 methylation possibly by regulating the expression of histone methyltransferases or MLL-complex members.

The regulation of Pak6 expression seemed independent of DNMT1-induced changes in H3K4me3 levels

As we detected a global increase in permissive H3K4 trimethylation, we asked whether the elevated *Pak6* expression observed after *Dnmt1* depletion is caused by an enhanced association of trimethylated H3K4 to the *Pak6* gene locus. To this end, we applied chromatin-immunoprecipitation (ChIP) with an H3K4me3-specific antibody. Due to low cell counts of *Hmx3*-Cre expressing POA cells in embryonic brains, we switched to neuroblastoma (N2a) cells, proven as reliable cell culture model [29]. Similar to POA-derived interneurons [29], N2a cells showed up-regulated *Pak6* expression upon *Dnmt1* depletion and a comparable increase in their morphological complexity (Supp. Figure 2). Additionally, *Dnmt1*-depleted N2a cells displayed a global increase in H3K4 trimethylation levels determined by fluorescence intensity measurements of *Dnmt1* siRNA and control-treated cells (Figure 1(E-G)).

To quantitatively assess the association of trimethylated H3K4 to the *Pak6* gene we performed qPCR of ChIP products of control and *Dnmt1* siRNA-treated N2a cells using specific primers for promoter-flanking and non-regulatory sites of the *Pak6* gene locus (Figure 1(H)). A promoter region in the *Gapdh* gene locus was used to validate the method, as *Gapdh* is often associated with H3K4me3 [67,68]. The qPCR results were normalized against the amount of input DNA and control IgG was used to display unspecific antibody binding properties. Under control conditions we detected a prominent association of H3K4me3 within the promoter flanking region (#1 and #2 in Figure 1(I,J)) similar to *Gapdh*, as well as within the non-regulatory region (#3 in Figure 1(I,J)). However, we did not observe any changes in H3K4me3 association upon *Dnmt1* depletion in all regions analyzed (Figure 1(I,J)). Therefore, our data suggest that the transcription of *Pak6* is not regulated by DNMT1-dependent changes in H3K4 trimethylation, even if other genes might be modulated that way, as suggested by the global
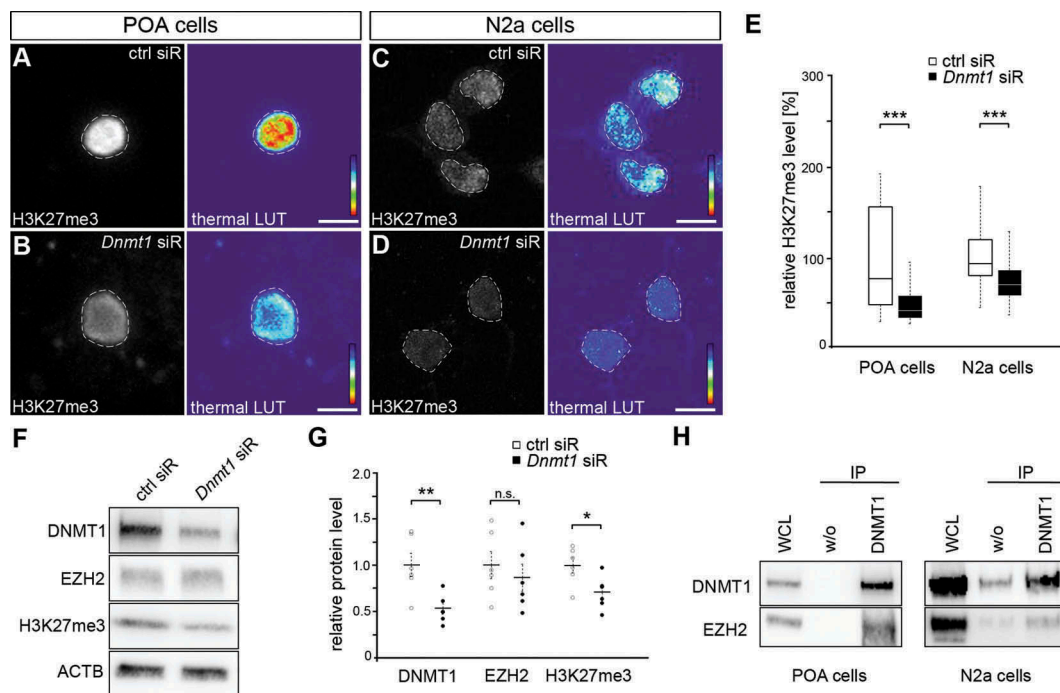
Figure 2. Repressive H3K27 trimethylation is reduced in *Dnmt1*-deficient cells. (A-E) Representative microphotographs of dissociated E16 (+ 2 DIV) POA cells (A, B) and N2a cells (C, D) treated either with control (A, C) or *Dnmt1* siRNA (B, D) and stained for H3K7me3, presented as fluorescence intensity in black/white code and as thermal color-code (thermal LUT). The mean grey value relative to control is quantified in E (n = 34 POA and 118 N2a cells for ctrl siRNA, n = 32 POA and 144 N2a cells for *Dnmt1* siRNA). (F, G) Protein levels of DNMT1, EZH2 and H3K27me3 in control and *Dnmt1* siRNA-treated N2a cells analyzed with Western blot (G), normalized to ACTB and quantified in relation to control (G; five individual experiments). (H) Co-immunoprecipitation with a DNMT1-specific antibody revealed a protein-protein interaction with EZH2 in E16 POA and N2a cell samples analyzed by Western blot (three individual experiments, two animals per experiment for POA cells). 'n' refers to the number of analyzed cells. $*P < 0.05; **P < 0.01;$ $***P < 0.001$; Student's t-test. Scale bars: 10 µm in (A-D). Ctrl, control; siR, siRNA; POA, preoptic area.

increase in H3K4me3 revealed by immunostaining after *Dnmt1* depletion (Figure 1(C,G)).

Repressive H3K27 trimethylation was decreased in Dnmt1-depleted neurons

To realize an optimal and fast transition between transcriptional states during development, genes are often marked bivalently by a co-occurrence of permissive H3K4me3 and repressive H3K27me3 modifications [69–74], and the ratio of H3K4me3 and H3K27me3 often decides about gene transcription [72]. H3K27 trimethylation is regulated by the polycomb repressor complex 2 (PCR2) through its core enzyme EZH2, and diverse effector proteins mediate complex stability and specificity [75–81]. Interestingly, fluorescence intensity measurements of H3K27me3 in both embryonic POA-derived interneurons as well as N2a cells, treated either with control or *Dnmt1* siRNA, revealed a global reduction of H3K27me3 upon *Dnmt1*

depletion (Figure 2(A-E)). This is in line with other studies showing diminished H3K27 trimethylation levels upon *Dnmt1* deletion as well as after inhibition of EZH2 [53,82–85].

It was reported that DNMT1 can affect H3K27me3 through the transcriptional control over genes encoding for members of the H3K27 trimethylation machinery like EZH2. However, we did not detect any transcriptional changes in PCR2-related transcripts between *Dnmt1* wild-type and knockout POA-derived interneurons of E16 mice (Supp. Figure 3A). In agreement with this, neither *Dnmt1* depletion by siRNA nor blocking the DNA methylating function of DNMT1 by RG108 treatment in cultured N2a cells resulted in reduced EZH2 protein levels (Figure 2(F,G); Supp. Figure 3 (B,C)). In contrast to EZH2, H3K27me3 levels were found reduced by Western blot analysis upon *Dnmt1* depletion (Figure 2(F,G)), confirming the results of the immunocytochemistry analysis (Figure 2(A-E)). However, blocking DNA methylation with RG108
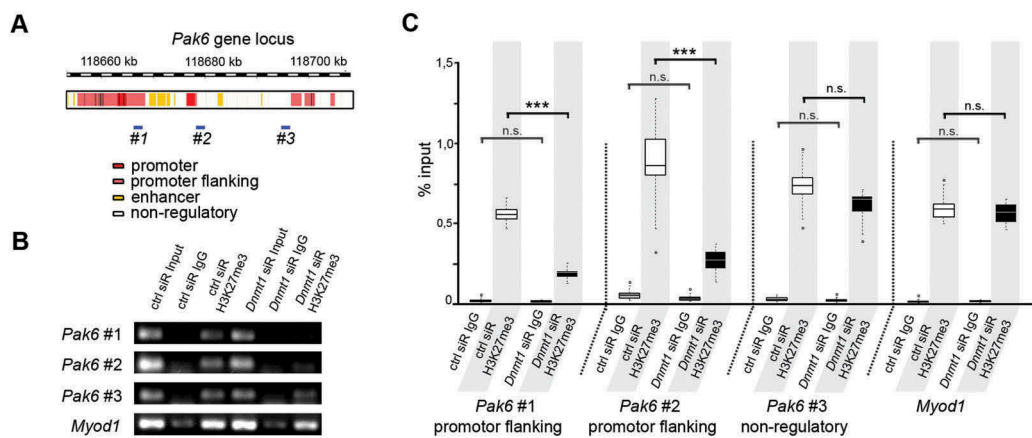
Figure 3. *Dnmt1*-depletion causes a reduced association of trimethylated H3K27 with *Pak6* regulatory regions. (A) Schematic illustration of the *Pak6* gene locus with promoter (red), promoter flanking (light red), enhancer (yellow) and non-regulatory (white) sites according to UCSC genome browser showing specific DNA primer positions (#1, #2, #3) in regulatory (#1, #2) and non-regulatory (#3) gene regions. (B, C) ChIP-analysis of control and *Dnmt1* siRNA-treated N2a cells with a H3K27me3-specific antibody shows the association of H3K27me3 to the indicated primer locations (#1–3 in A) in the *Pak6* gene (B), analyzed by quantitative PCR and normalized to the amount of input (C; three individual experiments with four technical replicates each). IgG controls indicate the amount of non-specifically bound DNA. ***$P < 0.001$; Student's t-test. Ctrl, control; siR, siRNA.

did not cause changes in the global H3K27me3 protein levels (Supp. Figure 3(B,C)). Together, these results indicate that DNMT1 modulates H3K27 trimethylation independently of the transcriptional control over PCR2 components like EZH2.

For non-neuronal cells direct interactions of DNMT1 and EZH2 at protein level are described to realize a repressive transcriptional state [52,82]. Indeed, co-immunoprecipitation experiments performed with isolated POA cells of E16 wild-type brains as well as N2a cells confirmed an interaction of DNMT1 and EZH2 in both cell types (Figure 2(H)). Thus, these data point to a DNMT1-dependent modulation of H3K27 trimethylation via protein-protein interaction with EZH2 in developing POA-derived interneurons and neuron-like cells.

DNMT1 represss Pak6 expression by promoting the association of repressive H3K27me3 marks in promoter flanking regions

To elucidate whether DNMT1-dependent modulation of H3K27me3 is involved in the regulation of *Pak6* expression, we next performed ChIP with a H3K27me3-specific antibody using control and

Dnmt1 siRNA-treated N2a cells. The immunoprecipitated DNA was quantitatively analyzed for *Pak6* gene fragments using the same primer as for H3K4me3 analysis directed against promoter-flanking regions as well as non-regulatory gene regions of *Pak6* (Figure 3(A)). Primer against a promoter region of *Myod1* were used as control, as this muscle-specific gene is usually strongly associated with H3K27me3 in neuronal cells to repress its transcription [86].

In control siRNA-treated cells, we detected a strong association of H3K27me3 at the promoter-flanking positions of the *Pak6* gene locus (Figure 3 (B,C), #1 and #2), as well as at the non-regulatory region (Figure 3(B,C), #3). Upon *Dnmt1* depletion, we found significantly decreased levels of H3K27me3 within the regulatory gene regions of the *Pak6* gene locus (Figure 3(B,C), #1 and #2). Apart from that, we did not detect any relevant changes within the non-regulatory site (Figure 3(B, C), #3). This reduced association of trimethylated H3K27 induced by *Dnmt1* depletion was in line with the observed increase in *Pak6* expression.

As an association of H3K27me3 near gene promoter regions often suppresses transcription of the respective genes [76,77,87], our results emphasize a
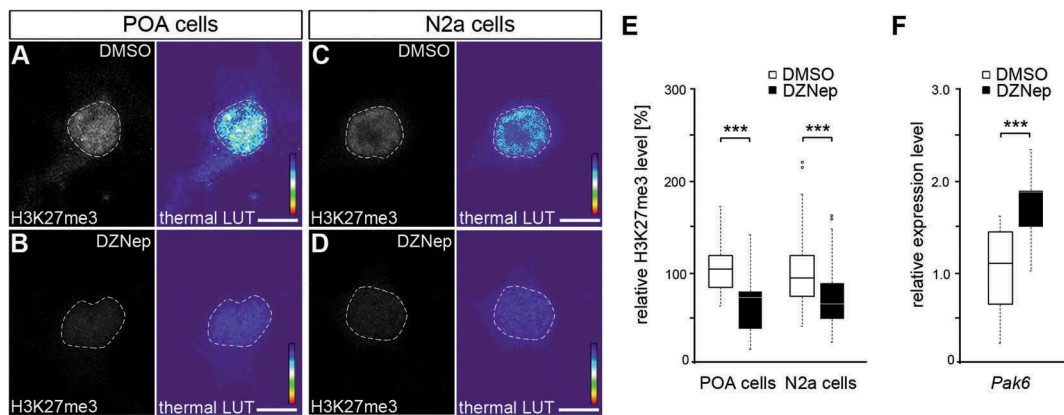
Figure 4. EZH2 inhibition by DZNep reduces global H3K27me3 levels and elevates *Pak6* gene expression. (A-E) Representative microphotographs of dissociated E16 (+ 2 DIV) POA cells (A, B) and N2a cells (C, D) treated either with DMSO (A, C) or the EZH2 inhibitor DZNep (B, D) and stained with a H3K7me3-specific antibody, shown as fluorescence intensity in black/white code and as thermal color-code (thermal LUT). The mean grey value is quantified relative to DMSO controls in E (n = 37 POA and 120 N2a cells for DMSO, n = 36 POA and 102 N2a cells for DZNep). (F) Quantitative PCR displays increased *Pak6* expression in DZNep-treated N2a cells compared to DMSO controls, normalized against *Rps29* and *Actb* (three individual experiments with four technical replicates each). 'n' refers to the number of analyzed cells. ***P < 0.001; Student's t-test.

DNMT1-dependent repression of *Pak6* transcription through the modulation of EZH2-mediated H3K27 trimethylation.

EZH2 inhibition lead to changes in morphology similar to the effects induced by Dnmt1 depletion

The experiments described so far indicated that DNMT1 represses *Pak6* expression through interactions with EZH2, thereby affecting H3K27me3 marks. To functionally verify the EZH2-dependent transcriptional regulation of *Pak6*, we treated cultured N2a cells with the inhibitor 3-Deazaneplanocin A (DZNep), shown to increase protein degradation of EZH2 [88,89]. In line with other studies [89–91], we detected decreased levels of global H3K27me3 compared to DMSO-treated controls in both, embryonic POA-derived primary neurons (Figure 4(A,B)) and N2a cells (Figure 4(C,D)) upon DZNep-mediated degradation of EZH2, as analyzed by intensity measurements of immunocytochemical stainings (Figure 4(E)). Furthermore, in comparison to DMSO controls quantitative measurements revealed enhanced *Pak6* expression after DZNep-induced EZH2 degradation (Figure 4(F)), confirming the relevance of this histone methyltransferase for the transcriptional control of *Pak6*.

A *Dnmt1* deletion-induced elevation of *Pak6* expression in migrating POA-derived interneurons

was shown to change their morphological characteristics from a polarized migratory shape to an atypical complex morphology reminiscent of mature interneurons. This was assessed by measuring the leading and trailing process length, neurite numbers as well as branching frequencies [29]. To validate whether EZH2 inhibition that caused increased *Pak6* expression induces similar effects, we analyzed the morphology of dissociated POA-derived interneurons and N2a cells treated with DZNep (Figure 5A-E). Consistent with previous studies, in which forced PAK6 expression was induced [29], DZNep treatment lead to a substantial increase in cellular complexity of both cell types, characterized by augmented lengths of non-leading processes and a higher branch point occurrence (Figure 5(A-E)). To directly control whether the elevated *Pak6* expression contributes to this gain in cellular complexity, depletion of *Pak6* with target-specific siRNA was achieved in DZNep and DMSO-treated cells and compared to control transfections. Indeed, *Pak6* siRNA treatment rescued the DZNep-induced defects in POA cell morphology (Figure 5(F,J)), indicating that *Pak6* expression regulation in neurons depends on EZH2-mediated repressive H3K27 trimethylation in regulatory gene regions.

Together, the results presented here demonstrate that DNMT1 acts in concert with histone modifying mechanisms in developing POA-derived interneurons. In particular, *Pak6*
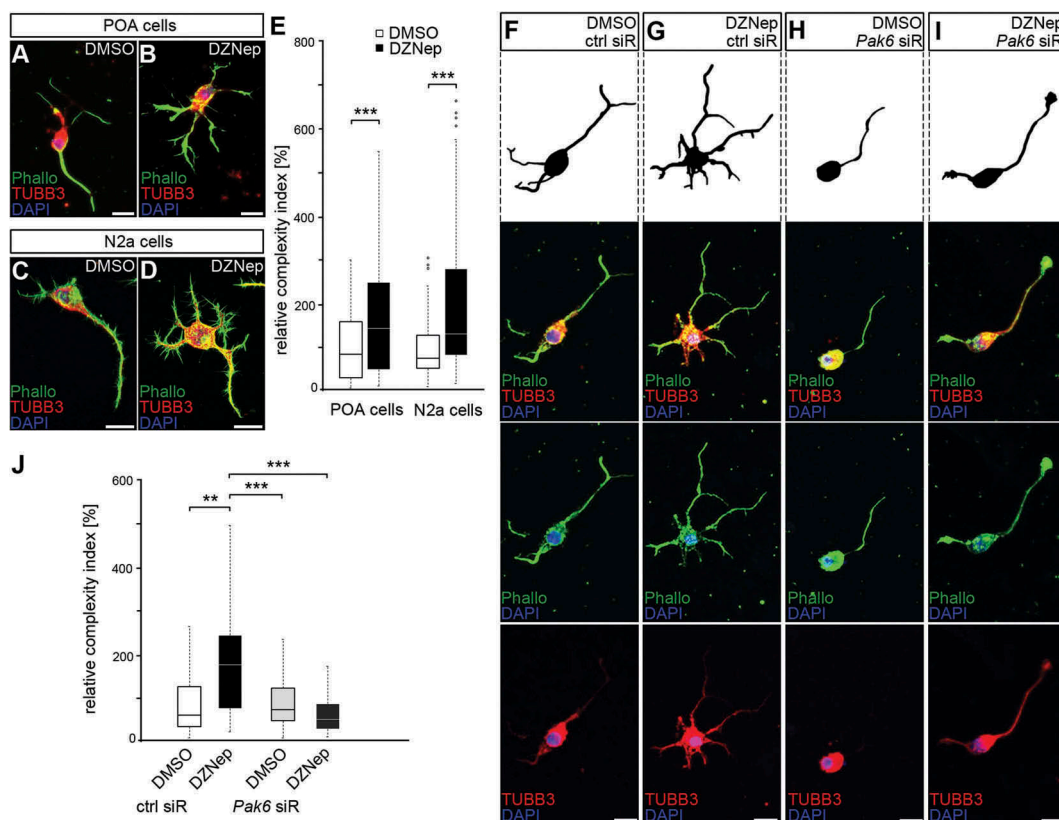
Figure 5. Enhanced *Pak6* expression induced by EZH2 inhibition results in increased morphological complexity. (A-E) Representative microphotographs of dissociated E16 (+ 2 DIV) POA cells (A, B) and N2a cells (C, D) treated either with DMSO (A, C) or DZNep (B, D) and stained against TUBB3 (green channel) with a specific antibody, ACTB (red channel) with fluorescently labeled phalloidin and DAPI (blue channel). Quantification of cell morphology is shown in (E) as complexity index relative to DMSO controls. The complexity index is a product of primary neurite number, the branch point number of the longest process and the ratio between longest process length and the mean length of all other neurites. (E; n = 52 POA and 85 N2a cells for DMSO, n = 69 POA and 93 N2a cells for DZNep). (F-J) Representative microphotographs of dissociated E16 (+ 2 div) POA cells treated either with DMSO (F, H) or DZNep (G, I) in addition to control (F, G) or *Pak6* siRNA (H, I), then stained against TUBB3 (green channel) with a specific antibody, ACTB (red channel) with fluorescently labeled phalloidin and DAPI (blue channel). The complexity index is quantified in (J) relative to DMSO + ctrl siRNA cell parameters (n = 39 POA cells for DMSO + ctrl siRNA, n = 43 POA cells for DZNep + ctrl siRNA, n = 51 POA cells for DMSO + Pak6 siRNA, n = 68 POA cells for DZNep + Pak6 siRNA). 'n' refers to the number of analyzed cells. $**P < 0.01$; $***P < 0.001$; Student's t-test. Ctrl, control; siR, siRNA; POA, preoptic area.

repression in immature interneurons seems to rely on a DNMT1-dependent modulation of repressive H3K27 trimethylations mediated by interactions between DNMT1 and EZH2.

Discussion

Developmental processes in neurons underlie a multifaceted epigenetic regulation triggering stage and cell type-specific transcriptional programs [92–95]. While stable gene repression potentially restricts cell fate, flexible and fast gene regulation allows the adaption to transient intrinsic and extrinsic cues [40–42]. DNMT-mediated DNA methylation was initially considered as a stable repressive mark and as a key mechanism for permanent gene silencing during development and over lifetime [96–99]. However, active and selective DNA demethylation processes enable dynamic DNA methylation and contribute to an adjustable transcriptional control in neuronal cell types [100–106]. Although, DNMT1 was classified as maintenance methyltransferase with a high affinity to hemimethylated DNA strands after replication [107–109], there are many studies reporting additional functions during post-mitotic neuronal development as well as in the adult brain [29,43,46,110–113].

In our previous study, we highlighted the function of DNMT1 in facilitating the migration and

survival of immature inhibitory interneurons in part by transcriptional repression of the gene coding for the serine/threonine-protein kinase PAK6 [29]. However, our data pointed to a DNA methylation-independent regulation of *Pak6* expression by DNMT1 [29]. In the present study, we provided evidence that the transcriptional control of *Pak6* relies on a DNMT1-dependent establishment of repressive histone marks through interactions with histone-modifying enzymes.

This is consistent with the results obtained by RNA and MeDIP sequencing of *Hmx3*-expressing *Dnmt1* wild-type and knockout POA cells, showing no correlation between transcriptional changes and alterations in gene methylation for many membrane-, cell shape- and protein phosphorylation-associated genes. Immature interneurons have to quickly adapt their morphology in regard to changing external guidance cues during their migration from their sites of origin in the basal telencephalon towards cortical targets [114–117]. Therefore, the expression of genes important for the composition and arrangement of cytoskeletal compartments as well as membrane-bound proteins like specific guidance receptors has to be rapidly adapted upon signal detection and integration [116,118–122]. Often, these processes are regulated by protein phosphorylation [123–126], which also necessitates a flexible regulation of respective protein kinases like the PAKs [47,127,128]. Although active DNA demethylation is shown to realize rapid activity-dependent transcriptional changes in post-mitotic neurons [101], DNA methylation and demethylation seem rather regulate temporally orchestrated programs in neurons facilitating subtype-specific differentiation and maturation over the developmental time course [129].

However, DNMT1 additionally appears to contribute to the transcriptional control of genes important for highly dynamic processes like cell shape modulation through distinct mechanisms apart from direct DNA methylation. Several studies already emphasize the relevance of non-canonical DNMT1 functions in regulating gene activity showing that the enzyme is also repressively active without its catalytic domain [130–132]. In addition to the transcriptional control over genes encoding for proteins involved in the methylation of histone tail amino acids, DNMT1 directly interacts with these proteins, thereby coordinately determining

the chromatin status and allowing for transient gene expression [50,51,133,134].

In agreement with this, we found elevated global H3K4me3 and diminished H3K27me3 levels upon *Dnmt1* depletion, proposing a function for DNMT1 in modulating these histone tail modifications in POA-derived interneurons. H3K4me3 marks, mostly detected at transcription start sites of gene promoters and other regulatory gene regions together with the RNA polymerase II [135–137], are strongly associated with active gene transcription [62]. In turn, H3K27me3 sites were predominantly found within inactive chromatin regions [76,77,87].

Consistent with changes in H3K4me3 levels, we found an elevated expression of components facilitating H3K4 trimethylation upon *Dnmt1* deletion by screening the RNA sequencing dataset published in Pensold et al., 2016 [29]. This included transcripts coding for the histone-lysine-N-methyltransferases (HKMT) KMT2D and KMT2G (SETD1B), which specifically perform mono- and tri-methylation at H3K4 [58–60]. Hence, altered expression of HKMT like KMT2D or KMT2G may facilitate DNA methylation-independent alterations in gene transcription in POA-derived *Dnmt1*-deficient interneurons.

Although we collected evidence for a DNMT1-mediated control of H3K4me3 marks, transcriptional levels of *Pak6* in immature POA-derived interneurons rather rely on a DNMT1-dependent regulation of H3K27 trimethylation. While associations of H3K4me3 with regulatory regions at the *Pak6* gene locus were observed, we did not detect an increase upon *Dnmt1* depletion, neither at regulatory nor non-regulatory *Pak6* gene sites. However, we can not exclude that more distanced regulatory regions up- or down-stream are possibly changed in their association with H3K4me3.

In contrast to H3K4me3, the association of repressive H3K27me3 histone marks in *Pak6* regulatory regions was diminished upon *Dnmt1* depletion consistent with the global decrease. This indicates that in addition to H3K4me3, DNMT1 affects trimethylation of H3K27 in neuronal cells and that *Pak6* expression is regulated through DNMT1-induced changes in H3K27me3 association. Comprehensive studies in mice analyzing methylated lysine residues of H3 already revealed a bivalent regulation of many developmental genes by permissive H3K4me3 and

repressive H3K27me3 residues adopting a 'winner-takes-all' principle [71,72,138]. That means, the decision about the transcriptional activity of these genes depends on the proportion of both histone marks.

Trimethylations at lysines 27 of histone 3 proteins are performed by the Polycomb repressor complex 2 (PCR2) [76,139], consisting of the core enzyme *enhancer of zeste* (EZH2) and diverse accessory components [77,78]. During early brain development, EZH2 is the main methyltransferase of PCR2 [79–81]. With neuronal maturation its expression decreases and the repressive function is taken over by EZH1 in a similar polycomb protein complex [140,141].

For non-neuronal cells, an interplay of DNMT1 and EZH2 was already shown [53,82,84,85,142–144] and the global decrease of H3K27me3 we detected in neurons with diminished *Dnmt1* expression is consistent with other studies [53,82,83]. Some studies suggest a modulation of DNMT1 function by EZH2, as it is found to bind and recruit the DNA methyltransferase to specific gene sites and to regulate DNA methylation properties [82,142–144]. Vice versa, a widespread H3K27me3 redistribution and the re-expression of Polycomb-target genes upon DNA hypomethylation is reported [83], suggesting that DNMT1 potentially acts upstream of EZH2. In this context, DNMT1 is already described to affect the expression of the Polycomb methyltransferase and other PCR2 components as well as H3K27 trimethylation [53,83–85]. Thereby, manipulation of DNMT1 function or expression induces an increased generation of miR-214, which targets *Ezh2* leading to its degradation [53,145,146]. MiR-214 is further suggested to support DNMT1 via a self-regulatory feedback mechanism, as it triggers the degradation of a DNMT1 repressor protein [146]. However, as EZH2 also targets miR-214 for gene silencing [145], more work needs to be done to uncover all aspects of the complex relationship between DNMT1, EZH2 and further regulatory components.

In contrast to studies in cancer cells [53,84], we neither detected changes in EZH2 expression nor in the expression of accessory PCR2 components upon *Dnmt1* depletion in POA interneurons and neuron-like N2a cells, although they revealed significantly diminished H3K27 trimethylation. Our data emphasize that in POA neurons and neurons-like N2a cells the H3K27me3 marks rather depend on the interaction of DNMT1 and EZH2 proteins than on DNMT1-dependent transcriptional control of PCR2 components.

How is the target-specificity of such complexes regulated? Recent studies highlight an important function of non-coding RNA derivatives in mediating EZH2 binding to specific gene regions [147]. For example, in a complex with DNMT1, the lncRNAs LINC00673 and HOXA-11-AS participate in the recruitment of EZH2 [148,149]. Thus, DNMT1 possibly modulates H3K27 trimethylation not only through the direct interaction with EZH2, but also via the assembly of further components like lncRNAs that in turn determine target specificity. Moreover, the demethylase LSD1 is found in a close relation to HOXA-11-AS and DNMT1, removing H3K4 methylation and contributing to gene silencing [149]. This supports the role of DNMT1 in mediating gene accessibility through the recruitment and regulation of many epigenetic key players and its involvement in bivalent gene regulation.

Among those genes regulated by DNMT1-EZH2 interactions, we also suspected *Pak6*, which was confirmed by chromatin-immunoprecipitation experiments and pharmacological inhibition of EZH2 with DZNep, inducing an up-regulation of *Pak6* gene transcription along with a down-regulation of H3K27 trimethylation. Similar to morphological alterations seen in *Dnmt1*-deficient cells [29], DZNep-treated POA neurons also displayed increasing cellular complexity mimicking the morphological phenotype of *Dnmt1*-deficient POA-derived interneurons. DZNep treatment was already shown to induce morphological alterations as it possibly affects the expression of many genes [150,151]. However, the siRNA-mediated downregulation of *Pak6* levels in DZNep-treated POA cells rescued their cell morphology, underlining our hypothesis of a DNMT1-dependent regulation of *Pak6* through EZH2-dependent alterations in H3K27 trimethylations.

Moreover, based on the simultaneous association of H3K27me3 and H3K4me3 at the investigated positions of the *Pak6* gene locus, we hypothesize a bivalent regulation of *Pak6* expression. Although H3K4me3 levels were not changed in *Dnmt1*-depleted cells, the reduced trimethylation of H3K27 might allow a fast up-regulation of *Pak6* expression due to a

proportional higher association of H3K4me3. This could facilitate transcriptional activity, which was already reported for several developmental genes [62]. This bivalent mechanism might be of relevance for the observed switch between the repressive *Pak6* gene state during interneuron migration in developing embryos and the increased transcription of *Pak6* in cortical interneurons of newborn pubs [29]. As PAK6 was reported to be important for neurite outgrowth during differentiation of excitatory neurons in the cortex [48], a 'switched-on' expression in interneurons that have reached their cortical target area would favor their maturation.

In conclusion, our study highlighted the importance of DNMT1 for regulating gene expression in immature interneurons via DNA methylation-independent mechanisms. Thereby, changes in repressive H3K27 trimethylation seem to rely on the interaction of DNMT1 with the PCR2 core histone methyltransferase EZH2. Moreover, our data revealed that *Pak6* regulatory gene regions are associated with both repressive H3K27me3 and permissive H3K4me3, proposing a bivalent regulation.

Material and methods

Animals

Wild-type mice on a C57BL/6 background were used for all experiments. All animal procedures were performed in strict compliance with the EU directives 86/609/EWG and 2007/526/EG guidelines for animal experiments and were approved by the local government (Thueringer Landesamt, Bad Langensalza, Germany). Animals were housed under 12 h light/dark conditions with *ad libitum* access to food and water.

Preparation of embryonic single cells from the POA

For the preparation of embryonic POA cells, timed pregnant mice were killed by an intraperitoneal injection of 50% chloral hydrate in phosphate-buffered saline (PBS; pH 7.4). Embryos were removed and decapitated, brains prepared and embedded in 4% low-melt agarose (Sigma-Aldrich). Coronal living brain sections (300 μm) from embryonic brains were prepared at the vibratome (VT1000S, Leica) at 4°C in Krebs' buffer (126 mM NaCl, 2.5 mM, KCL, 1.2 mM NaH_2PO_4, 1.2 mM $MgCl_2$, 2.1 mM $CaCl_2$, 10 mM D-Glucose, 12.5 mM $NaHCO_3$). Slices were collected in post holding buffer (Krebs' buffer with 1 M HEPES, 100 U/mL penicillin and 100 μg/mL streptomycin). POA domains were prepared under visual control. Brain tissue was incubated with 0.025% trypsin (Thermo Fisher Scientific) in Hank's balanced salt solution (Invitrogen) for 17 min at 37°C. Cells were then dissociated by trituration and cell aggregates were removed by filtering through a nylon gauze (200 μm). Single cells were seeded at densities of 300 cells/mm^2 on coverslips (Ø 12 mm) coated with 19 μg/μL laminin (Sigma-Aldrich) and 5 μg/μL poly-L-lysine (Sigma-Aldrich) in Grey´s balanced salt solution (GBSS) and incubated in DMEM/F12 (1:1, Invitrogen), 10% fetal bovine serum (FBS; Biowest), 100 U/mL penicillin (Gibco), 100 g/mL streptomycin (Gibco), 0.4 mM L-glutamine (Gibco), 0.15% D-glucose at 37°C, 5% CO_2, and 95% humidity for 1 day *in vitro* (div) before further treatment. For co-immunoprecipitation, POA cells were washed in PBS and pelleted by centrifugation (1000 g at 4°C for 5 min) before further treatment.

N2a cell culture

Neuro-2a (N2a) cells were cultured in DMEM (Invitrogen), 2% FBS (Biowest), 100 U/mL penicillin (Gibco), 100 g/mL streptomycin (Gibco) at 37°C, 5% CO_2, and 95% humidity. When reaching 75% confluence, N2a cells were mechanically dissociated and divided by the ratio 1:4. Before further treatment, N2a cells were seeded at densities of 100 cells/mm^2 on coverslips (Ø 12 mm) coated with 19 μg/μL laminin (Sigma-Aldrich) und 5 μg/μL poly-L-lysine (Sigma-Aldrich) in GBSS and incubated in DMEM (Thermo Fisher Scientific), 2% FBS, 100 U/mL penicillin, 100 g/mL streptomycin at 37°C, 5% CO_2, and 95% humidity for 24 h.

Transfection of primary neuron culture and N2a cells with siRNA

Transfection of dissociated embryonic POA cells of C57BL/6 wild-type mice and N2a cells with siRNA was performed via lipofection using Lipofectamine

RNAiMAX (Thermo Fisher Scientific), according to the manufacturer's protocol and as described in Zimmer et al. (2011) [152]. Mouse *Dnmt1* siRNA oligos (50 nM) or mouse *Pak6* siRNA oligos (50 nM), containing a pool of at least three target-specific 19–25 nt siRNAs to knockdown gene expression (*Dnmt1* siRNA sc-35,203; *Pak6* siRNA sc-44,879; Santa Cruz Biotechnology) or 50 nM control siRNA (BLOCK-iT Alexa Fluor red/green fluorescent oligo; Invitrogen) were applied for 5 h in antibiotic-free Opti-MEM I Reduced Serum Medium (Thermo Fisher Scientific) at 37°C, 5% CO_2, and 95% humidity. Then, primary cells were incubated in DMEM/F12 (1:1, Invitrogen), 10% FBS (Biowest), 100 U/mL penicillin (Gibco), 100 g/mL streptomycin (Gibco), 0.4 mM L-glutamine (Gibco), 0.15% D-glucose and N2a cells in DMEM (Invitrogen), 2% FBS (Biowest), 100 U/mL penicillin (Gibco), 100 g/mL streptomycin (Gibco) for 24 h at 37°C, 5% CO_2, and 95% humidity.

DZNep and RG108 treatment

To inhibit EZH2 function, dissociated POA cells were treated with 1.5 μM 3-Deazaneplanocin A (DZNep, Sigma-Aldrich) in DMEM/F12 (1:1, Invitrogen), 10% FBS, 100 U/mL penicillin, 100 g/mL streptomycin, 0.4 mM L-glutamine, 0.15% D-glucose. N2a cells were treated with 100 nM DZNep (Sigma-Aldrich) in DMEM (Invitrogen), 2% FBS, 100 U/mL penicillin, 100 g/mL streptomycin for 24 h at 37°C, 5% CO_2, and 95% humidity. N-phthalyl-L-tryptophan (20 μM, RG108, Sigma-Aldrich) was used to block DNA methylation in N2a cells cultured in DMEM (Thermo Fisher Scientific), 2% FBS, 100 U/mL penicillin, 100 g/mL streptomycin for 24 h at 37° C, 5% CO_2, and 95% humidity. As control, POA and N2a cells were treated with dimethyl sulfoxide (DMSO).

RNA preparation and expression analysis

For RNA expression analysis, siRNA- or DZNep-treated N2a cells cultured in 6 well plates were harvested in Trizol Reagent (Life Technologies), frozen and stored at −20°C. N2a cells were subjected to standard RNA isolation procedure in Trizol Reagent (Life

Technologies), digested with RNase-free DNase (Qiagen) and quality and RNA quantities were measured with the NanoDrop™1000 (Thermo Fisher Scientific). RNA was analyzed in a one-step qRT-PCR using the SuperScript III Platinum SYBR Green One-Step qRT-PCR Kit (Thermo Fisher Scientific) with the following primer sequences (indicated as 5′ to 3′; fw, forward; rev, reverse): *Dnmt1* fw TGAGC ATCGATGAGGAGATG, *Dnmt1* rev CGCAT GGAACATCATCTGAC, *Pak6* fw CTGTACG CTACTGAGGTGGA, *Pak6* rev GTACCAG CATCCGATCCAGG, *Rps29* fw GAAGTTCG GCCAGGGTTCC, *Rps29* rev GAAGCCTATG TCCTTCGCGT, *bAct* fw AGAGGGAAATC GTGCGTGAC, *bAct* rev CAATAGTGATGA CCTGGCCGT.

Immunocytochemistry and immunohistochemistry

POA and N2a cells cultured on coverslips and used for immunohistochemical stainings were fixed with 4% PFA for 10 min and stored in PBS at 4°C. Immunocytochemistry of fixed dissociated cells was performed as previously described in Zimmer et al. (2011 [152]). Briefly, cells were washed in PBS with 0.1% Triton X-100 and treated with the blocking reagent (4% bovine serum albumin in PBS with 0.1% Triton X-100) for 30 min at room temperature. Primary antibody incubation was performed for 3 h and secondary antibody incubation for 1 h at room temperature in blocking solution. Incubation with Alexa Fluor™ 488 Phalloidin (Thermo Fisher Scientific) to stain F-actin was performed according to the manufacturer's guidelines. Cells were stained with DAPI for 5 min at room temperature. Following primary antibodies were used: rabbit anti-β-III-tubulin (TUBB3, Sigma-Aldrich; 1:500), rabbit anti-H3K4me3 (Abcam, 1:500), rabbit anti-H3K27me3 (Millipore, 1:500). Cy3 goat anti-rabbit IgG (1:1000; Jackson Laboratory) was used as secondary antibody.

Co-immunoprecipitation

For analysis of protein interactions, N2a cells cultured in 6 well plates were harvested and similar to

dissociated POA cells pelleted by centrifugation (1000 g at 4°C for 5 min). Cell pellets were resuspended in RIPA buffer (50 mM Tris/HCl pH 8.0, 150 mM NaCl, 0.5% NP-40, 0.1% SDS, 0.1% sodium deoxycholate, 1 mM PMSF, 500 μM leupeptine) and lysed for 10 min on ice with subsequent treatment in an ultrasonic water bath (Sonorex super 10P, Bandelin) for 1 min. Lysates were centrifuged for 20 min at 20,000 g and 4°C. The supernatant (whole cell lysate) was applied for co-immunoprecipitation. Five percent of the supernatant was boiled for 10 min at 95°C in 4x sample buffer (200 mM Tris pH 6.8, 4% SDS, 10% β-mercaptoethanol, 40% glycerol, 0.002% bromophenol blue) and stored at −20°C used later as positive control for protein incidence in the lysate.

For co-immunoprecipitation, protein A agarose beads (Millipore) were washed in RIPA buffer and incubated at 4°C for 1 h with 4 μg antibody directed against rabbit anti-DNMT1 (CosmoBio). Control beads were incubated without antibody. Empty binding sites were blocked by adding 45 μg bovine serum albumin (Serva). After 1 h incubation, the supernatant was removed and whole cell lysates were added to the beads for 2 h at 4°C. Then, beads were washed six times in RIPA buffer, boiled for 10 min at 95°C in 4x sample buffer (200 mM Tris pH 6.8, 4% SDS, 10% β-mercaptoethanol, 40% glycerol, 0.002% bromophenol blue) and stored at −20°C for protein detection.

Protein preparation and expression analysis

To quantitatively assess protein expression, N2a cells were cultured in 6 well plates and harvested after 24 h of siRNA or RG108 treatment, washed in PBS and pelleted by centrifugation (1000 g at 4°C for 5 min). N2a cell pellets were lysed for 1 h on ice in lysis buffer containing 0.1 M Na_2HPO_4, 0.1 M NaH_2PO_4, 5 mM EDTA, 2 mM $MgCl_2$, 0.1 mM phenylmethylsulphonyl fluoride (PMSF, Serva), 500 μM Leupeptin (Serva) and 0.1% 3-[(3-cholamidopropyl) dimethylammonium]-1-propanesulfonate (CHAPS, Carl Roth). Cell lysates were treated for 1 min in an ultrasonic water bath (Sonorex super 10P, Bandelin) and centrifuged for 20 min at 20,000 g and 4°C. Supernatants were collected in new tubes and protein concentration was determined using the NanoDropTM1000

(Thermo Fisher Scientific). Lysates with a protein amount of 30 μg were boiled at 95°C for 10 min in 4x sample buffer containing 200 mM Tris pH 6.8, 4% SDS, 10% β-mercaptoethanol, 40% glycerol and 0.002% bromophenol blue and were stored at −20°C.

In 4x sample buffer frozen protein samples were separated on a ready-to-use 4–12% gradient gel (Serva) using 1x SDS-running buffer (Laemmli buffer, Serva) following manufacturer's instructions. For transfer of proteins to a nitrocellulose membrane in a semi-dry blot procedure a Towbin blotting kit (Serva) was used following the manufacturer's instructions. Subsequently, the membranes were blocked in 1x BlueBlock-reagent (Serva) for 1 h. Incubation with the following primary antibodies occurred over night: rabbit-anti-DNMT1 (CosmoBio, 1:1000), rabbit-anti-EZH2 (CellSignaling, 1:1000), rabbit-anti-H3K27me3 (Millipore, 1:1000), mouse-anti-β-actin (Abcam, 1:5000). The following secondary antibodies coupled to horseradish peroxidase (HRP) were applied for 1 h: sheep anti-mouse (GE Healthcare, 1:4000), donkey anti-rabbit (GE Healthcare, 1:4000). Membranes were washed after each incubation step three times for 5 min in TBS-T buffer (25 mM Tris/HCl pH 7.5, 137 mM NaCl, 2.7 mM KCl, 0.05% Tween-20). Chemo-luminescent detection of protein bands was performed at the blot documentation system ImageQuant LAS4000 (GE Healthcare) after applying the HRP substrate solution (Serva). Protein levels were normalized to β-actin.

Chromatin-immunoprecipitation and quantitative PCR

For chromatin-immunoprecipitation, N2a cells with a confluence of 75% were transfected with siRNA in 10 cm well plates. Twenty-four hours after transfection, N2a cells were washed with 37°C pre-warmed PBS and cross-linking of protein-DNA interactions was performed in 1% formaldehyde in PBS. The reaction was terminated by adding 0.125 M glycine. Cells were washed with PBS including 1 mM PMSF, 1 μg/mL aprotinine, 1 μg/mL pepstatine A (all from Serva), harvested with a cell scraper, aliquoted with a cell number of 1×10^6 cells per tube and centrifuged for 5 min at 1000 g at 4°C. Cell pellets were frozen in liquid

nitrogen and stored at −80°C before further treatment.

Protein-DNA cross-linked N2a cell pellets were resuspended and lysed in 50 mM Tris-HCl pH 8.1, 10 mM EDTA pH 8.0, 1% SDS including protease inhibitors (1 mM PMSF, 1 µg/ml aprotinine, 1 µg/ml pepstatine A; all from Serva) for 10 min at 4°C. DNA fragmentation was performed in an ultrasonic water bath (Sonorex super 10P, Bandelin) at 4°C with 30 cycles at 100% power setting and 30 s break between each cycle. After centrifugation for 10 min with 13.000 g at 4°C, supernatant was diluted in ChIP dilution buffer (16.7 mM Tris-HCl pH 8.1, 167 mM NaCl, 1.2 mM EDTA pH 8.0, 1.1% Triton X-100, 0.01% SDS) including protease inhibitors (1 mM PMSF, 1 µg/ml aprotinine, 1 µg/ml pepstatine A; all from Serva). 1% was taken as input control and stored at −20°C. To reduce unspecific binding to the agarose beads, probes were incubated for 30 min at 4°C with 3% protein A agarose/salmon sperm DNA (50% slurry; Merck Millipore). After centrifugation (1 min, 1000 g, 4°C), supernatant was incubated with 4 µg/mL antibody for 12 h at 4°C. Following antibodies were used for precipitation: rabbit anti-H3K4me3 (Abcam), rabbit anti-H3K27me3 (Millipore) and rabbit anti-IgG (Abcam). For detection of antibody-bound DNA fragments, probes were incubated for 1 h at 4°C with 3% protein A agarose/salmon sperm DNA (50% slurry; Merck Millipore). After centrifugation (1 min, 1000 g, 4°C), agarose pellets were washed for 5 min each with following solutions: *low salt immune complex*-wash buffer (20 mM Tris-HCl pH 8.1, 150 mM NaCl, 2 mM EDTA pH 8.0, 1% Triton X-100, 0.1% SDS), *high salt immune complex*-wash buffer (20 mM Tris-HCl pH 8.1, 500 mM NaCl, 2 mM EDTA pH 8.0, 1% Triton X-100, 0.1% SDS), *LiCl immune complex-wash* buffer (16.7 mM Tris-HCl pH 8.1, 250 mM LiCl, 1 mM EDTA pH 8.0, 1% sodium deoxycholate, 1% IGEPAL CA630) and 2 x TE buffer (10 mM Tris-HCl pH 8.1, 1 mM EDTA pH 8.0). For elution of DNA, pelleted agarose was incubated with elution buffer (1% SDS, 0.1 M NaHCO₃) for 15 min at room temperature. The supernatant was collected in a new tube after centrifugation (1 min, 1000 g, 4°C). The elution was repeated. Protein-DNA cross-linking of the eluate and input control probes were removed for 4 h at 65°C with 200 mM NaOH. Finally, proteins were digested for 1 h at 45°C in 10 mM EDTA, 40 mM Tris-HCl pH 6.5 und 20 µg/µl proteinase K (Merck Millipore). DNA was precipitated with standard phenol-chloroform isoamyl alcohol (25:24:1) extraction and purified with the DNA Clean & Concentrator-5 Kit (Zymo Research) according to the manufacturer's guidelines.

To quantitatively asses the amount of specific DNA fragments, primer-specific pre-amplification of probes was performed in the T-gradient PCR Cycler (Bio-Rad) for 20 cycles prior quantitative analysis with the Real-Time PCR-System qTOWER3/G (Analytik Jena). For both PCR reactions the innuMIX qPCR MasterMix SyGreen qPCR Kit (Analytik Jena) was used according to the manufacturer's guidelines. Following primer sequences were used (indicated as 5′ to 3′; fw, forward; rev, reverse): *Pak6-1* fw TCTC ACTCTCAGAAGCCAGG, *Pak6-1* rev AGCGT AGATCAGAGTGGGTG, *Pak6-2* fw ACACT GTGCTTCTCCCTAGG, *Pak6-2* rev TTCT CTCCGCTCCTTTCTCC, *Pak6-3* fw CGCTG CTGAAGTTCTTCTGG, *Pak6-3* rev GGCCCTTC TTACCGTCAGAT. Normalization of DNA content was performed according to the percent-input method in relation to the analyzed input probes [153].

Microscopy and data analysis

Fluorescent images were either taken with the inverted confocal laser scanning microscope TCS SP5 (Leica) or with the inverted Axio Cellobserver Z1 fluorescence microscope with a MosaiX module and Apotome (Carl Zeiss Microscopy). Photographs were analyzed with Fiji software (Schindelin, 2012). For fluorescence intensity measurement, each experimental design was imaged at one particular microscope with same settings regarding exposure time and light intensity at the CellObserver Z1, or laser power, gain and spectral settings at Zeiss SP5. Fluorescence intensity measurement of the cell nucleus of was applied for the H3K4me3 and H3K27me3 staining. Background correction was performed. Mean fluorescent intensity of the *Dnmt1* siRNA- or DZNep-treated cells was normalized to control siRNA- or dimethyl sulfoxide (DMSO)-treated cells. Quantitative

RNA results were analyzed by ΔCt method and presented in relation to control samples.

The dataset of the RNA and MeDIP-analysis performed and published in Pensold et al., 2016 [29] was used for the analysis presented here. Here, FAC-sorted cells of transgenic mice on the C57BL/6 background including *Hmx3-Cre/tdTomato/Dnmt1* wild-type as well as *Hmx3-Cre/tdTomato/Dnmt1 loxP2* mice were used. The transgenic mice were established by crossing the *Hmx3*-Cre line (obtained from Oscar Marin, King's College, London, UK and described in Gelman et al. 2009 [28]) with the *tdTomato* transgenic reporter mice (obtained from Christian Hübner, University Hospital Jena, Germany, and described in Madisen et al. 2010 [154]), and *Dnmt1 LoxP2* mice (B6;129Sv-Dnmt1tm4Jae/J, Jaenisch laboratory, Whitehead Institute, USA). Cre-mediated deletion leads to out-of-frame splicing from exon 3 to exon 6 of the *Dnmt1* gene, resulting in a null allele [155]. Data analysis was performed as described in Pensold et al., 2016 [29].

Photoshop CC was applied for image illustration. Significance was analyzed with two-tailed Student's t-test. Significance levels: *P* value < 0.05 *; *P* value < 0.01 **; *P* value < 0.001 ***. If not stated differently, experiments were repeated three times.

Authors´ contribution

JS: designed and performed experiments, data analysis, figure illustration, conceptual design of the study, wrote the manuscript; **CB**: performed experiments, manuscript correction; **CS**: performed experiments, data analysis, assisted in writing the manuscript; **AH**: data analysis; **DP**: data analysis, manuscript correction; **GZ**, conceptual design of the study, wrote the manuscript.

Disclosure statement

No potential conflict of interest was reported by the authors.

Funding

ORCID

Daniel Pensold 🔸 http://orcid.org/0000-0001-8685-1356
Geraldine Zimmer-Bensch 🔸 http://orcid.org/0000-0002-8894-8079

References

1. Zhou S, Yu Y. Synaptic E-I balance underlies efficient neural coding. Front Neurosci. 2018;12:46. PubMed PMID: 29456491; PubMed Central PMCID: PMC5801300.
2. Hennequin G, Agnes EJ, Vogels TP. Inhibitory plasticity: balance, control, and codependence. Annu Rev Neurosci. 2017 Jul 25;40:557–579.
3. Sprekeler H. Functional consequences of inhibitory plasticity: homeostasis, the excitation-inhibition balance and beyond. Curr Opin Neurobiol. 2017 Apr;43:198–203. PubMed PMID: 28500933.
4. Tatti R, Haley MS, Swanson OK, et al. Neurophysiology and Regulation of the Balance Between Excitation and Inhibition in Neocortical Circuits. Biol Psychiatry. 2017 May 15;81(10):821–831. PubMed PMID: 27865453; PubMed Central PMCID: PMC5374043.
5. Kepecs A, Fishell G. Interneuron cell types are fit to function. Nature. 2014 Jan 16;505(7483):318–326. . PubMed PMID: 24429630; PubMed Central PMCID: PMC4349583.
6. Tremblay R, Lee S, Rudy B. GABAergic Interneurons in the Neocortex: from Cellular Properties to Circuits. Neuron. 2016 Jul 20;91(2):260–292. . PubMed PMID: 27477017; PubMed Central PMCID: PMC4980915.
7. Rubenstein JL, Merzenich MM. Model of autism: increased ratio of excitation/inhibition in key neural systems. Genes Brain Behav. 2003 Oct;2(5):255–267. PubMed PMID: 14606691.
8. Levitt P, Eagleson KL, Powell EM. Regulation of neocortical interneuron development and the implications for neurodevelopmental disorders. Trends Neurosci. 2004 Jul;27(7):400–406. . PubMed PMID: 15219739.
9. Levitt P. Disruption of interneuron development. PubMed PMID: 16201992 Epilepsia. 2005;46Suppl 7:22–28.
10. Rossignol E. Genetics and function of neocortical GABAergic interneurons in neurodevelopmental disorders. Neural Plast. 2011;2011:649325. PubMed PMID: 21876820; PubMed Central PMCID: PMC3159129.
11. Rubenstein JL. Annual Research Review: development of the cerebral cortex: implications for neurodevelopmental disorders. J Child Psychol Psychiatry. 2011 Apr;52(4):339–355. . PubMed PMID: 20735793; PubMed Central PMCID: PMC3429600.
12. Chattopadhyaya B, Cristo GD. GABAergic circuit dysfunctions in neurodevelopmental disorders. Front Psychiatry. 2012;3:51. PubMed PMID: 22666213; PubMed Central PMCID: PMC3364508.

13. Goulburn AL, Stanley EG, Elefanty AG, et al. Generating GABAergic cerebral cortical interneurons from mouse and human embryonic stem cells. Stem Cell Res. 2012 May;8(3):416–426. PubMed PMID: 22280980.

14. Marin O. Interneuron dysfunction in psychiatric disorders. Nat Reviews Neurosci. 2012 Jan 18;13(2):107–120. . PubMed PMID: 22251963.

15. Volk DW, Matsubara T, Li S, et al. Deficits in transcriptional regulators of cortical parvalbumin neurons in schizophrenia. Am J Psychiatry. 2012 Oct;169 (10):1082–1091. PubMed PMID: 22983435; PubMed Central PMCID: PMC3513625.

16. Ye H, Kaszuba S. Inhibitory or excitatory? Optogenetic interrogation of the functional roles of GABAergic interneurons in epileptogenesis. J Biomed Sci. 2017 Dec 5;24(1):93. . PubMed PMID: 29202749; PubMed Central PMCID: PMC5715558.

17. Wonders CP, Anderson SA. The origin and specification of cortical interneurons. Nat Reviews Neurosci. 2006 Sep;7(9):687–696. . PubMed PMID: 16883309.

18. Druga R. Neocortical inhibitory system. Folia Biol (Krakow). 2009;55(6): 201–217. PubMed PMID: 20163769.

19. Gelman DM, Marin O. Generation of interneuron diversity in the mouse cerebral cortex. Eur J Neurosci. 2010 Jun;31(12):2136–2141. . PubMed PMID: 20529125.

20. Sultan KT, Brown KN, Shi SH. Production and organization of neocortical interneurons. Front Cell Neurosci. 2013 Nov 21;7:221.

21. Laclef C, Metin C. Conserved rules in embryonic development of cortical interneurons. Semin Cell Dev Biol. 2017 Sep 14. PubMed PMID: 28918121. doi:10.1016/j.semcdb.2017.09.017

22. Wichterle H, Garcia-Verdugo JM, Herrera DG, et al. Young neurons from medial ganglionic eminence disperse in adult and embryonic brain. Nat Neurosci. 1999 May;2(5):461–466. PubMed PMID: 10321251.

23. Anderson SA, Marin O, Horn C, et al. Distinct cortical migrations from the medial and lateral ganglionic eminences. Development. 2001 Feb;128(3):353–363. PubMed PMID: 11152634.

24. Wichterle H, Turnbull DH, Nery S, et al. In utero fate mapping reveals distinct migratory pathways and fates of neurons born in the mammalian basal forebrain. Development. 2001 Oct;128(19):3759–3771. PubMed PMID: 11585802.

25. Flames N, Pla R, Gelman DM, et al. Delineation of multiple subpallial progenitor domains by the combinatorial expression of transcriptional codes. J Neuroscience: Official Journal Soc Neurosci. 2007 Sep 05;27(36):9682–9695. PubMed PMID: 17804629; PubMed Central PMCID: PMC4916652.

26. Corbin JG, Butt SJ. Developmental mechanisms for the generation of telencephalic interneurons. Dev Neurobiol. 2011 Aug;71(8):710–732. . PubMed PMID: 21485015.

27. Marin O. Cellular and molecular mechanisms controlling the migration of neocortical interneurons. Eur J Neurosci. 2013 Jul;38(1):2019–2029. . PubMed PMID: 23651101.

28. Gelman DM, Martini FJ, Nobrega-Pereira S, et al. The embryonic preoptic area is a novel source of cortical GABAergic interneurons. J Neuroscience: Official Journal Soc Neurosci. 2009 Jul 22;29(29):9380–9389. PubMed PMID: 19625528.

29. Pensold D, Symmank J, Hahn A, et al. The DNA methyltransferase 1 (DNMT1) control the shape and dynamics of migrating POA-derived interneurons fated for the murine cerebral cortex. Cereb Cortex. 2016 Dec 1;27 (12):5696–5714. PubMed PMID: 29117290.

30. Symmank J, Goelling V, Gerstmann K, et al. The Transcription Factor LHX1 Regulates the Survival and Directed Migration of POA-derived Cortical Interneurons. Cereb Cortex. 2018. doi:10.1093/cercor/bhy063.

31. Nadarajah B, Parnavelas JG. Modes of neuronal migration in the developing cerebral cortex. Nat Reviews Neurosci. 2002 Jun;3(6):423–432. . PubMed PMID: 12042877.

32. Marin O, Rubenstein JL. A long, remarkable journey: tangential migration in the telencephalon. Nat Reviews Neurosci. 2001 Nov;2(11):780–790. . PubMed PMID: 11715055.

33. Metin C, Baudoin JP, Rakic S, et al. Cell and molecular mechanisms involved in the migration of cortical interneurons. Eur J Neurosci. 2006 Feb;23(4):894–900. PubMed PMID: 16519654.

34. Miller MW. Relationship of the time of origin and death of neurons in rat somatosensory cortex: barrel versus septal cortex and projection versus local circuit neurons. J Comp Neurol. 1995 Apr 24;355(1):6–14. . PubMed PMID: 7636014.

35. Southwell DG, Paredes MF, Galvao RP, et al. Intrinsically determined cell death of developing cortical interneurons. Nature. 2012 Nov 01;491(7422):109–113. PubMed PMID: 23041929; PubMed Central PMCID: PMC3726009.

36. Uribe E, Wix R. Neuronal migration, apoptosis and bipolar disorder. Rev Psiquiatr Salud Ment. 2012 Apr-Jun;5(2):127–133. . PubMed PMID: 22854584.

37. Denaxa M, Neves G, Rabinowitz A, et al. Modulation of Apoptosis Controls Inhibitory Interneuron Number in the Cortex. Cell Rep. 2018 Feb 13;22(7):1710–1721. PubMed PMID: 29444425.

38. Hu JS, Vogt D, Sandberg M, et al. Cortical interneuron development: a tale of time and space. Development. 2017 Nov 1;144(21):3867–3878. PubMed PMID: 29089360; PubMed Central PMCID: PMC5702067.

39. Symmank J, Zimmer G. Regulation of neuronal survival by DNA methyltransferases. Neural Regeneration Research. 2017 Nov;12(11):1768–1775. . PubMed PMID: 29239313.

40. Jaenisch R, Bird A. Epigenetic regulation of gene expression: how the genome integrates intrinsic and

environmental signals. Nat Genet. 2003 Mar;33:245–254. PubMed PMID: 12610534.

41. Feng J, Fouse S, Fan G. Epigenetic regulation of neural gene expression and neuronal function. Pediatr Res. 2007 May;61(5 Pt 2):58R–63R. . PubMed PMID: 17413844.

42. Cholewa-Waclaw J, Bird A, Von Schimmelmann M, et al. The Role of Epigenetic Mechanisms in the Regulation of Gene Expression in the Nervous System. J Neuroscience: Official Journal Soc Neurosci. 2016 Nov 09;36(45):11427–11434. PubMed PMID: 27911745; PubMed Central PMCID: PMC5125210.

43. Akbarian S, Beeri MS, Haroutunian V. Epigenetic Determinants of Healthy and Diseased Brain Aging and Cognition. In: JAMA Neurology. 2013. doi:10.1001/jamaneurol.2013.1459

44. Fagiolini M, Jensen CL, Champagne FA. Epigenetic influences on brain development and plasticity. Curr Opin Neurobiol. 2009 Apr;19(2):207–212. . PubMed PMID: 19545993; PubMed Central PMCID: PMC2745597.

45. Mitchell AC, Bharadwaj R, Whittle C, et al. The genome in three dimensions: a new frontier in human brain research. Biol Psychiatry. 2014 Jun 15;75 (12):961–969. PubMed PMID: 23958183; PubMed Central PMCID: PMC3925763.

46. Lv J. The Epigenetic Switches for Neural Development and Psychiatric Disorders. J Genet Genomics. 2013 Jul 20;40(7):339–346. PubMed PMID: 23876774..

47. Kumar R, Sanawar R, Li X, et al. Structure, biochemistry, and biology of PAK kinases. Gene. 2017 Mar 20;605:20–31. PubMed PMID: 28007610; PubMed Central PMCID: PMC5250584.

48. Civiero L, Cirnaru MD, Beilina A, et al. Leucine-rich repeat kinase 2 interacts with p21-activated kinase 6 to control neurite complexity in mammalian brain. J Neurochem. 2015 Dec;135(6):1242–1256. PubMed PMID: 26375402; PubMed Central PMCID: PMC4715492.

49. Civiero L, Cogo S, Kiekens A, et al. PAK6 Phosphorylates 14-3-3gamma to Regulate Steady State Phosphorylation of LRRK2. Front Mol Neurosci. 2017;10:417. PubMed PMID: 29311810; PubMed Central PMCID: PMC5735978.

50. Du J, Johnson LM, Jacobsen SE, et al. DNA methylation pathways and their crosstalk with histone methylation. Nature Reviews Molecular Cell Biology. 2015 Sep;16(9):519–532. PubMed PMID: 26296162; PubMed Central PMCID: PMC4672940.

51. Rose NR, Klose RJ. Understanding the relationship between DNA methylation and histone lysine methylation. Biochim Biophys Acta. 2014 Dec;1839(12):1362–1372. . PubMed PMID: 24560929; PubMed Central PMCID: PMC4316174.

52. Vire E, Brenner C, Deplus R, et al. The Polycomb group protein EZH2 directly controls DNA methylation. Nature. 2006 Feb 16;439(7078):871–874. PubMed PMID: 16357870.

53. So AY, Jung JW, Lee S, et al. DNA methyltransferase controls stem cell aging by regulating BMI1 and EZH2 through microRNAs. PloS One. 2011 May 10;6(5): e19503. PubMed PMID: 21572997; PubMed Central PMCID: PMC3091856.

54. Jenuwein T, Allis CD. Translating the histone code. Science. 2001 Aug 10;293(5532):1074–1080. . PubMed PMID: 11498575.

55. Bannister AJ, Kouzarides T. Regulation of chromatin by histone modifications. Cell Res. 2011 Mar;21 (3):381–395. . PubMed PMID: 21321607; PubMed Central PMCID: PMC3193420.

56. Lawrence M, Daujat S, Schneider R. Lateral Thinking: how Histone Modifications Regulate Gene Expression. Trends in Genetics: TIG. 2016 Jan;32(1):42–56. . PubMed PMID: 26704082.

57. Harr JC, Gonzalez-Sandoval A, Gasser SM. Histones and histone modifications in perinuclear chromatin anchoring: from yeast to man. EMBO Rep. 2016 Feb;17(2):139–155. . PubMed PMID: 26792937; PubMed Central PMCID: PMC4783997.

58. Guo C, Chen LH, Huang Y, et al. KMT2D maintains neoplastic cell proliferation and global histone H3 lysine 4 monomethylation. Oncotarget. 2013 Nov;4 (11):2144–2153. PubMed PMID: 24240169; PubMed Central PMCID: PMC3875776.

59. Froimchuk E, Jang Y, Ge K. Histone H3 lysine 4 methyltransferase KMT2D. Gene. 2017 Sep 05;627:337–342.

60. Brici D, Zhang Q, Reinhardt S, et al. Setd1b, encoding a histone 3 lysine 4 methyltransferase, is a maternal effect gene required for the oogenic gene expression program. Development. 2017 Jul 15;144(14):2606–2617. PubMed PMID: 28619824.

61. Lee JH, Tate CM, You JS, et al. Identification and characterization of the human Set1B histone H3-Lys4 methyltransferase complex. J Biol Chem. 2007 May 4;282(18):13419–13428. PubMed PMID: 17355966.

62. Eissenberg JC, Shilatifard A. Histone H3 lysine 4 (H3K4) methylation in development and differentiation. Dev Biol. 2010 Mar 15;339(2):240–249. . PubMed PMID: 19703438; PubMed Central PMCID: PMC3711867.

63. Shen E, Shulha H, Weng Z, et al. Regulation of histone H3K4 methylation in brain development and disease. Philosophical Transactions of the Royal Society of London Series B, Biological Sciences. 2014 Sep 26;369 (1652). PubMed PMID: 25135975; PubMed Central PMCID: PMC4142035.

64. Vallianatos CN, Iwase S. Disrupted intricacy of histone H3K4 methylation in neurodevelopmental disorders. PubMed PMID: 26077434; PubMed Central PMCID: PMC4501478 Epigenomics. 2015;73:503–519.

65. Nakagawa T, Xiong Y. X-linked mental retardation gene CUL4B targets ubiquitylation of H3K4 methyltransferase component WDR5 and regulates neuronal

gene expression. Mol Cell. 2011 Aug 05;43(3):381–391. . PubMed PMID: 21816345; PubMed Central PMCID: PMC3230935.

66. Nakagawa T, Xiong Y. Chromatin regulation by CRL4 E3 ubiquitin ligases: CUL4B targets WDR5 ubiquitylation in the nucleus. Cell Cycle. 2011 Dec 15;10 (24):4197–4198. . PubMed PMID: 22107965; PubMed Central PMCID: PMC5442879.

67. Wang P, Lin C, Smith ER, et al. Global analysis of H3K4 methylation defines MLL family member targets and points to a role for MLL1-mediated H3K4 methylation in the regulation of transcriptional initiation by RNA polymerase II. Mol Cell Biol. 2009 Nov;29 (22):6074–6085. PubMed PMID: 19703992; PubMed Central PMCID: PMC2772563.

68. Bhandare R, Schug J, Le Lay J, et al. Genome-wide analysis of histone modifications in human pancreatic islets. Genome Res. 2010 Apr;20(4):428–433. PubMed PMID: 20181961; PubMed Central PMCID: PMC2847745.

69. Bernstein BE, Mikkelsen TS, Xie X, et al. A bivalent chromatin structure marks key developmental genes in embryonic stem cells. Cell. 2006 Apr 21;125(2):315–326. PubMed PMID: 16630819.

70. Mikkelsen TS, Ku M, Jaffe DB, et al. Genome-wide maps of chromatin state in pluripotent and lineage-committed cells. Nature. 2007 Aug 02;448(7153):553–560. PubMed PMID: 17603471; PubMed Central PMCID: PMC2921165.

71. Voigt P, Tee WW, Reinberg D. A double take on bivalent promoters. Genes Dev. 2013 Jun 15;27 (12):1318–1338. . PubMed PMID: 23788621; PubMed Central PMCID: PMC3701188.

72. Cui P, Liu W, Zhao Y, et al. Comparative analyses of H3K4 and H3K27 trimethylations between the mouse cerebrum and testis. Genomics, Proteomics & Bioinformatics. 2012 Apr;10(2):82–93. PubMed PMID: 22768982; PubMed Central PMCID: PMC5054206.

73. Barski A, Cuddapah S, Cui K, et al. High-resolution profiling of histone methylations in the human genome. Cell. 2007 May 18;129(4):823–837. PubMed PMID: 17512414.

74. Burney MJ, Johnston C, Wong KY, et al. An epigenetic signature of developmental potential in neural stem cells and early neurons. Stem Cells. 2013 Sep;31 (9):1868–1880. PubMed PMID: 23712654.

75. Hontelez S, Van Kruijsbergen I, Georgiou G, et al. Embryonic transcription is controlled by maternally defined chromatin state. Nat Commun. 2015 Dec 18;6:10148. PubMed PMID: 26679111; PubMed Central PMCID: PMC4703837.

76. Boros J, Arnoult N, Stroobant V, et al. Polycomb repressive complex 2 and H3K27me3 cooperate with H3K9 methylation to maintain heterochromatin protein 1alpha at chromatin. Mol Cell Biol. 2014 Oct 1;34 (19):3662–3674. PubMed PMID: 25047840; PubMed Central PMCID: PMC4187721.

77. Jiao L, Liu X. Structural basis of histone H3K27 tri-methylation by an active polycomb repressive complex 2. Science. 2015 Oct 16;350(6258):aac4383. . PubMed PMID: 26472914; PubMed Central PMCID: PMC5220110.

78. Chittock EC, Latwiel S, Miller TC, et al. Molecular architecture of polycomb repressive complexes. Biochem Soc Trans. 2017 Feb 8;45(1):193–205. PubMed PMID: 28202673; PubMed Central PMCID: PMC5310723.

79. Feng X, Juan AH, Wang HA, et al. Polycomb Ezh2 controls the fate of GABAergic neurons in the embryonic cerebellum. Development. 2016 Jun 1;143 (11):1971–1980. PubMed PMID: 27068104; PubMed Central PMCID: PMC4920161.

80. Zhao L, Li J, Ma Y, et al. Ezh2 is involved in radial neuronal migration through regulating Reelin expression in cerebral cortex. Sci Rep. 2015 Oct 26;5:15484. PubMed PMID: 26499080; PubMed Central PMCID: PMC4620455.

81. Pereira JD, Sansom SN, Smith J, et al. Ezh2, the histone methyltransferase of PRC2, regulates the balance between self-renewal and differentiation in the cerebral cortex. Proc Natl Acad Sci U S A. 2010 Sep 7;107 (36):15957–15962. PubMed PMID: 20798045; PubMed Central PMCID: PMC2936600.

82. Ning X, Shi Z, Liu X, et al. DNMT1 and EZH2 mediated methylation silences the microRNA-200b/a/ 429 gene and promotes tumor progression. Cancer Lett. 2015 Apr 10;359(2):198–205. PubMed PMID: 25595591.

83. Reddington JP, Perricone SM, Nestor CE, et al. Redistribution of H3K27me3 upon DNA hypomethylation results in de-repression of Polycomb target genes. Genome Biol. 2013 Mar 25;14(3):R25. PubMed PMID: 23531360; PubMed Central PMCID: PMC4053768.

84. Purkait S, Sharma V, Kumar A, et al. Expression of DNA methyltransferases 1 and 3B correlates with EZH2 and this 3-marker epigenetic signature predicts outcome in glioblastomas. Exp Mol Pathol. 2016 Apr;100(2):312–320. PubMed PMID: 26892683.

85. Wu J, Tang Q, Yang L, et al. Interplay of DNA methyltransferase 1 and EZH2 through inactivation of Stat3 contributes to beta-elemene-inhibited growth of naso-pharyngeal carcinoma cells. Sci Rep. 2017 Mar 30;7 (1):509. 10.1038/s41598-017-00626-6. PubMed PMID: 28360411; PubMed Central PMCID: PMC5428779.

86. Wang AH, Zare H, Mousavi K, et al. The histone chaperone Spt6 coordinates histone H3K27 demethylation and myogenesis. EMBO J. 2013 Apr 17;32 (8):1075–1086. PubMed PMID: 23503590; PubMed Central PMCID: PMC3630356.

87. Conway E, Healy E, Bracken AP. PRC2 mediated H3K27 methylations in cellular identity and cancer. Curr Opin Cell Biol. 2015 Dec;37:42–48. PubMed PMID: 26497635.

88. Tan J, Yang X, Zhuang L, et al. Pharmacologic disruption of Polycomb-repressive complex 2-mediated gene repression selectively induces apoptosis in cancer cells. Genes Dev. 2007 May 1;21(9):1050–1063. PubMed PMID: 17437993; PubMed Central PMCID: PMC1855231.

89. Girard N, Bazille C, Lhuissier E, et al. 3-Deazaneplanocin A (DZNep), an inhibitor of the histone methyltransferase EZH2, induces apoptosis and reduces cell migration in chondrosarcoma cells. PloS One. 2014;9(5):e98176. PubMed PMID: 24852755; PubMed Central PMCID: PMC4031152.

90. Nakagawa S, Sakamoto Y, Okabe H, et al. Epigenetic therapy with the histone methyltransferase EZH2 inhibitor 3-deazaneplanocin A inhibits the growth of cholangiocarcinoma cells. Oncol Rep. 2014 Feb;31(2):983–988. PubMed PMID: 24337160.

91. Kikuchi J, Takashina T, Kinoshita I, et al. Epigenetic therapy with 3-deazaneplanocin A, an inhibitor of the histone methyltransferase EZH2, inhibits growth of non-small cell lung cancer cells. Lung Cancer. 2012 Nov;78(2):138–143. PubMed PMID: 22925699; PubMed Central PMCID: PMC3472089.

92. Geiman TM, Robertson KD. Chromatin remodeling, histone modifications, and DNA methylation-how does it all fit together?. PubMed PMID: 12244565 J Cell Biochem. 2002;872:117–125.

93. Fuks F. DNA methylation and histone modifications: teaming up to silence genes. Curr Opin Genet Dev. 2005 Oct;15(5):490–495. . PubMed PMID: 16098738.

94. Vaissiere T, Sawan C, Herceg Z. Epigenetic interplay between histone modifications and DNA methylation in gene silencing. Mutat Res. 2008 Jul-Aug;659(1–2):40–48. . PubMed PMID: 18407786.

95. Cedar H, Bergman Y. Linking DNA methylation and histone modification: patterns and paradigms. Nat Reviews Genet. 2009 May;10(5):295–304. . PubMed PMID: 19308066.

96. Lande-Diner L, Zhang J, Ben-Porath I, et al. Role of DNA methylation in stable gene repression. J Biol Chem. 2007 Apr 20;282(16):12194–12200. PubMed PMID: 17311920.

97. Hashimshony T, Zhang J, Keshet I, et al. The role of DNA methylation in setting up chromatin structure during development. Nat Genet. 2003 Jun;34(2):187–192. PubMed PMID: 12740577.

98. Razin A, Cedar H. DNA methylation and gene expression. Microbiol Rev. 1991 Sep;55(3):451–458. PubMed PMID: 1943996; PubMed Central PMCID: PMC372829.

99. Moore LD, Le T, Fan G. DNA methylation and its basic function. Neuropsychopharmacology: Official Publication Am Coll Neuropsychopharmacol. 2013 Jan;38(1):23–38. . PubMed PMID: 22781841; PubMed Central PMCID: PMC3521964.

100. Reik W, Dean W, Walter J. Epigenetic reprogramming in mammalian development. Science. 2001 Aug 10;293 (5532):1089–1093. . PubMed PMID: 11498579.

101. Martinowich K, Hattori D, Wu H, et al. DNA methylation-related chromatin remodeling in activity-dependent BDNF gene regulation. Science. 2003 Oct 31;302 (5646):890–893. PubMed PMID: 14593184.

102. Weaver IC, Cervoni N, Champagne FA, et al. Epigenetic programming by maternal behavior. Nat Neurosci. 2004 Aug;7(8):847–854. PubMed PMID: 15220929.

103. Weaver IC, Champagne FA, Brown SE, et al. Reversal of maternal programming of stress responses in adult offspring through methyl supplementation: altering epigenetic marking later in life. J Neuroscience: Official Journal Soc Neurosci. 2005 Nov 23;25 (47):11045–11054. PubMed PMID: 16306417.

104. Miller CA, Sweatt JD. Covalent modification of DNA regulates memory formation. Neuron. 2007 Mar 15;53 (6):857–869. . PubMed PMID: 17359920.

105. Feng J, Zhou Y, Campbell SL, et al. Dnmt1 and Dnmt3a maintain DNA methylation and regulate synaptic function in adult forebrain neurons. Nat Neurosci. 2010 Apr;13(4):423–430. PubMed PMID: 20228804; PubMed Central PMCID: PMC3060772.

106. Gavin DP, Chase KA, Sharma RP. Active DNA demethylation in post-mitotic neurons: a reason for optimism. Neuropharmacology. 2013 Dec;75:233–245. PubMed PMID: 23958448; PubMed Central PMCID: PMC3864977.

107. Hermann A, Goyal R, Jeltsch A. The Dnmt1 DNA-(cytosine-C5)-methyltransferase methylates DNA processively with high preference for hemimethylated target sites. J Biol Chem. 2004 Nov 12;279(46):48350–48359. . PubMed PMID: 15339928.

108. Hirasawa R, Chiba H, Kaneda M, et al. Maternal and zygotic Dnmt1 are necessary and sufficient for the maintenance of DNA methylation imprints during pre-implantation development. Genes Dev. 2008 Jun 15;22 (12):1607–1616. PubMed PMID: 18559477; PubMed Central PMCID: PMC2428059.

109. Bashtrykov P, Jankevicius G, Smarandache A, et al. Specificity of Dnmt1 for methylation of hemimethylated CpG sites resides in its catalytic domain. Chem Biol. 2012 May 25;19(5):572–578. PubMed PMID: 22633409.

110. Chestnut BA, Chang Q, Price A, et al. Epigenetic regulation of motor neuron cell death through DNA methylation. J Neuroscience: Official Journal Soc Neurosci. 2011 Nov 16;31(46):16619–16636. PubMed PMID: 22090490; PubMed Central PMCID: PMC3238138.

111. Kadriu B, Guidotti A, Chen Y, et al. DNA methyltransferases1 (DNMT1) and 3a (DNMT3a) colocalize with GAD67-positive neurons in the GAD67-GFP mouse

brain. J Comp Neurol. 2012 Jun 15;520(9):1951–1964. PubMed PMID: 22134929; PubMed Central PMCID: PMC3890098.

112. Hutnick LK, Golshani P, Namihira M, et al. DNA hypomethylation restricted to the murine forebrain induces cortical degeneration and impairs postnatal neuronal maturation. Hum Mol Genet. 2009 Aug 01;18(15):2875–2888. PubMed PMID: 19433415; PubMed Central PMCID: PMC2706688.

113. Fan G, Martinowich K, Chin MH, et al. DNA methylation controls the timing of astrogliogenesis through regulation of JAK-STAT signaling. Development. 2005 Aug;132(15):3345–3356. PubMed PMID: 16014513.

114. Hatanaka Y, Zhu Y, Torigoe M, et al. From migration to settlement: the pathways, migration modes and dynamics of neurons in the developing brain. Proc Japan Acad Ser B, Phys Biological Sciences. 2016;92 (1):1–19. PubMed PMID: 26755396; PubMed Central PMCID: PMC4880546.

115. Guo J, Anton ES. Decision making during interneuron migration in the developing cerebral cortex. Trends Cell Biol. 2014 Jun;24(6):342–351. . PubMed PMID: 24388877; PubMed Central PMCID: PMC4299592.

116. Peyre E, Silva CG, Nguyen L. Crosstalk between intracellular and extracellular signals regulating interneuron production, migration and integration into the cortex. Front Cell Neurosci. 2015;9:129. PubMed PMID: 25926769; PubMed Central PMCID: PMC4396449.

117. Hernandez-Miranda LR, Parnavelas JG, Chiara F. Molecules and mechanisms involved in the generation and migration of cortical interneurons. ASN Neuro. 2010 Mar 31;2(2):e00031. . PubMed PMID: 20360946; PubMed Central PMCID: PMC2847827.

118. Friocourt G, Liu JS, Antypa M, et al. Both doublecortin and doublecortin-like kinase play a role in cortical interneuron migration. J Neuroscience: Official Journal Soc Neurosci. 2007 Apr 04;27(14):3875–3883. PubMed PMID: 17409252.

119. Britto JM, Johnston LA, Tan SS. The stochastic search dynamics of interneuron migration. Biophys J. 2009 Aug 05;97(3):699–709. . PubMed PMID: 19651028; PubMed Central PMCID: PMC2718142.

120. Martini FJ, Valiente M, Lopez Bendito G, et al. Biased selection of leading process branches mediates chemotaxis during tangential neuronal migration. Development. 2009 Jan;136(1):41–50. PubMed PMID: 19060332.

121. Steinecke A, Gampe C, Nitzsche F, et al. DISC1 knockdown impairs the tangential migration of cortical interneurons by affecting the actin cytoskeleton. Front Cell Neurosci. 2014;8:190. PubMed PMID: 25071449; PubMed Central PMCID: PMC4086047.

122. Tielens S, Huysseune S, Godin JD, et al. Elongator controls cortical interneuron migration by regulating actomyosin dynamics. Cell Res. 2016 Oct;26(10):1131–1148. PubMed PMID: 27670698; PubMed Central PMCID: PMC5113307.

123. Maekawa M, Ishizaki T, Boku S, et al. Signaling from rho to the actin cytoskeleton through protein kinases ROCK and LIM-kinase. Science. 1999 Aug 6;285(5429):895–898. PubMed PMID: WOS:000081860900051; English.

124. Schmandke A, Schmandke A, Strittmatter SM. ROCK and Rho: biochemistry and neuronal functions of rho-associated protein kinases. Neuroscientist. 2007 Oct;13 (5):454–469. . PubMed PMID: WOS:000249763300013; English.

125. Besson A, Gurian-West M, Schmidt A, et al. p27(Kip1) modulates cell migration through the regulation of RhoA activation. Genes Dev. 2004 Apr 15;18(8):862–876. PubMed PMID: WOS:000221028500003; English.

126. Godin JD, Thomas N, Laguesse S, et al. p27(KiP1) Is a Microtubule-Associated Protein that Promotes Microtubule Polymerization during Neuron Migration. Dev Cell. 2012 Oct 16;23(4):729–744. PubMed PMID: WOS:000310036200010; English.

127. Zhao ZS, Manser E. PAK and other Rho-associated kinases - effectors with surprisingly diverse mechanisms of regulation. Biochem J. 2005 Mar 1;386:201–214.

128. Zhao ZS, Manser E. PAK family kinases: physiological roles and regulation. Cell Logist. 2012 Apr 01;2(2):59–68. . PubMed PMID: 23162738; PubMed Central PMCID: PMC3490964.

129. Sharma A, Klein SS, Barboza L, et al. Principles Governing DNA Methylation during Neuronal Lineage and Subtype Specification. J Neuroscience: Official Journal Soc Neurosci. 2016 Feb 3;36(5):1711–1722. PubMed PMID: 26843651; PubMed Central PMCID: PMC4737779.

130. Clements EG, Mohammad HP, Leadem BR, et al. DNMT1 modulates gene expression without its catalytic activity partially through its interactions with histone-modifying enzymes. Nucleic Acids Res. 2012 May;40(10):4334–4346. PubMed PMID: 22278882; PubMed Central PMCID: PMC3378872.

131. Milutinovic S, Brown SE, Zhuang Q, et al. DNA methyltransferase 1 knock down induces gene expression by a mechanism independent of DNA methylation and histone deacetylation. J Biol Chem. 2004 Jul 2;279 (27):27915–27927. PubMed PMID: 15087453.

132. Espada J, Peinado H, Lopez-Serra L, et al. Regulation of SNAIL1 and E-cadherin function by DNMT1 in a DNA methylation-independent context. Nucleic Acids Res. 2011 Nov;39(21):9194–9205. PubMed PMID: 21846773; PubMed Central PMCID: PMC3241660.

133. Kondo Y. Epigenetic cross-talk between DNA methylation and histone modifications in human cancers. Yonsei Med J. 2009 Aug 31;50(4):455–463. . PubMed PMID: 19718392; PubMed Central PMCID: PMC2730606.

134. Cheng X. Structural and functional coordination of DNA and histone methylation. Cold Spring Harb Perspect Biol. 2014 Aug 1;6(8). PubMed PMID: 25085914; PubMed Central PMCID: PMC4107986. doi:10.1101/cshperspect.a018747.

135. Barrera LO, Li Z, Smith AD, et al. Genome-wide mapping and analysis of active promoters in mouse embryonic stem cells and adult organs. Genome Res. 2008 Jan;18(1):46–59. PubMed PMID: 18042645; PubMed Central PMCID: PMC2134779.

136. Guenther MG, Jenner RG, Chevalier B, et al. Global and Hox-specific roles for the MLL1 methyltransferase. Proc Natl Acad Sci U S A. 2005 Jun 14;102(24):8603–8608. PubMed PMID: 15941828; PubMed Central PMCID: PMC1150839.

137. Guenther MG, Levine SS, Boyer LA, et al. A chromatin landmark and transcription initiation at most promoters in human cells. Cell. 2007 Jul 13;130(1):77–88. PubMed PMID: 17632057; PubMed Central PMCID: PMC3200295.

138. Li F, Wan M, Zhang B, et al. Bivalent Histone Modifications and Development. Curr Stem Cell Res Ther. 2018;13(2):83–90. PubMed PMID: 28117006.

139. Van Kruijsbergen I, Hontelez S, Veenstra GJ. Recruiting polycomb to chromatin. Int J Biochem Cell Biol. 2015 Oct;67:177–187. PubMed PMID: 25982201; PubMed Central PMCID: PMC4564301.

140. Shen X, Liu Y, Hsu YJ, et al. EZH1 mediates methylation on histone H3 lysine 27 and complements EZH2 in maintaining stem cell identity and executing pluripotency. Mol Cell. 2008 Nov 21;32(4):491–502. PubMed PMID: 19026780; PubMed Central PMCID: PMC2630502.

141. Margueron R, Li G, Sarma K, et al. Ezh1 and Ezh2 maintain repressive chromatin through different mechanisms. Mol Cell. 2008 Nov 21;32(4):503–518. PubMed PMID: 19026781; PubMed Central PMCID: PMC3641558.

142. Hoffmann MJ, Engers R, Florl AR, et al. Expression changes in EZH2, but not in BMI-1, SIRT1, DNMT1 or DNMT3B are associated with DNA methylation changes in prostate cancer. Cancer Biol Ther. 2007 Sep;6(9):1403–1412. PubMed PMID: 18637271.

143. Fiskus W, Buckley K, Rao R, et al. Panobinostat treatment depletes EZH2 and DNMT1 levels and enhances decitabine mediated de-repression of JunB and loss of survival of human acute leukemia cells. Cancer Biol Ther. 2009 May;8(10):939–950. PubMed PMID: 19279403; PubMed Central PMCID: PMC2775142.

144. Wu X, Gong Y, Yue J, et al. Cooperation between EZH2, NSPc1-mediated histone H2A ubiquitination and Dnmt1 in HOX gene silencing. Nucleic Acids Res. 2008 Jun;36(11):3590–3599. PubMed PMID: 18460542; PubMed Central PMCID: PMC2441805.

145. Juan AH, Kumar RM, Marx JG, et al. Mir-214-dependent regulation of the polycomb protein Ezh2 in skeletal muscle and embryonic stem cells. Mol Cell. 2009 Oct 9;36(1):61–74. PubMed PMID: 19818710; PubMed Central PMCID: PMC2761245.

146. Chen BF, Suen YK, Gu S, et al. A miR-199a/miR-214 self-regulatory network via PSMD10, TP53 and DNMT1 in testicular germ cell tumor. Sci Rep. 2014 Sep 18;4:6413. PubMed PMID: 25231260; PubMed Central PMCID: PMC4166711.

147. Holoch D, Margueron R. Mechanisms Regulating PRC2 Recruitment and Enzymatic Activity. Trends Biochem Sci. 2017 Jul;42(7):531–542. . PubMed PMID: 28483375.

148. Ba MC, Long H, Cui SZ, et al. Long noncoding RNA LINC00673 epigenetically suppresses KLF4 by interacting with EZH2 and DNMT1 in gastric cancer. Oncotarget. 2017 Nov 10;8(56):95542–95553. PubMed PMID: 29221147; PubMed Central PMCID: PMC5707041.

149. Sun M, Nie F, Wang Y, et al. LncRNA HOXA11-AS Promotes Proliferation and Invasion of Gastric Cancer by Scaffolding the Chromatin Modification Factors PRC2, LSD1, and DNMT1. Cancer Res. 2016 Nov 1;76(21):6299–6310. PubMed PMID: 27651312.

150. Hatta M, Naganuma K, Kato K, et al. 3-Deazaneplanocin A suppresses aggressive phenotype-related gene expression in an oral squamous cell carcinoma cell line. Biochem Biophys Res Commun. 2015 Dec 4–11;468(1–2):269–273. PubMed PMID: 26505792.

151. Choudhury SR, Balasubramanian S, Chew YC, et al. (-)-Epigallocatechin-3-gallate and DZNep reduce polycomb protein level via a proteasome-dependent mechanism in skin cancer cells. Carcinogenesis. 2011 Oct;32(10):1525–1532. PubMed PMID: 21798853; PubMed Central PMCID: PMC3179425.

152. Zimmer G, Rudolph J, Landmann J, et al. Bidirectional ephrinB3/EphA4 signaling mediates the segregation of medial ganglionic eminence- and preoptic area-derived interneurons in the deep and superficial migratory stream. J Neuroscience: Official Journal Soc Neurosci. 2011 Dec 14;31(50):18364–18380. PubMed PMID: 22171039.

153. Haring M, Offermann S, Danker T, et al. Chromatin immunoprecipitation: optimization, quantitative analysis and data normalization. Plant Methods. 2007 Sep 24;3:11. PubMed PMID: 17892552; PubMed Central PMCID: PMC2077865.

154. Madisen L, Zwingman TA, Sunkin SM, et al. A robust and high-throughput Cre reporting and characterization system for the whole mouse brain. Nat Neurosci. 2010 Jan;13(1):133–140. PubMed PMID: 20023653; PubMed Central PMCID: PMC2840225.

155. Jackson-Grusby L, Beard C, Possemato R, et al. Loss of genomic methylation causes p53-dependent apoptosis and epigenetic deregulation. Nat Genet. 2001 Jan;27(1):31–39. PubMed PMID: 11137995.